physica status solidi pss a
www.pss-a.com

Recent Progress of Deep Ultraviolet Photodetectors using Amorphous Gallium Oxide Thin Films

Huili Liang, Zuyin Han, and Zengxia Mei**

Deep ultraviolet (UV) photodetectors have wide applications both in civil and military fields. Many materials have been explored to realize deep UV photodetection. Amorphous gallium oxide (a-GaO$_x$), as a member of transparent amorphous oxide semiconductors (TAOSs), has attracted a great deal of attention due to its ultrawide bandgap and scalable synthesis at room temperature. Plenty of researches have been focused on this topic in recent years. Herein, the latest progresses in the preparation methods of a-GaO$_x$ using radio-frequency sputtering, pulsed laser deposition, atomic layer deposition, and other deposition techniques are summarized. Dependence of the stoichiometry, crystallinity, optical, electrical, and morphological properties on different preparation parameters and doping/alloying elements is tentatively discussed, as well as those deep UV photodetectors based on a-GaO$_x$ and related thin films. Finally, a short summary with further possible investigations is provided for a better understanding and development of a-GaO$_x$ materials and photodetectors.

1. Introduction

Ultraviolet (UV) photodetectors (PDs), as pivotal elements in modern optoelectronic devices, have attracted increasing research interest in recent years because of their wide applications both in civil and military fields such as confidential space communication, flame detection, imaging, and missile warning systems.[1] Gallium oxide is a desirable candidate for deep UV photodetection due to its suitable ultrawide bandgap (≈4.5 to 4.9 eV) without the necessity of alloying process.[2,3] It is reported that crystalline gallium oxide has five phases (α, β, γ, δ and ε) and β phase is the most stable.[4] Many kinds of crystalline gallium oxide UV PDs including bulk, thin films, and nanostructures have been demonstrated and summarized in several review articles recently.[5–8]

According to common understanding of semiconductors, properties of crystalline materials with limited defects are usually superior compared with their amorphous counterparts. For example, the performance of solar cells or transistors using crystalline Si is better than amorphous ones because the carrier mobility of crystalline Si is about 200 cm^2 V^{-1} s^{-1}, which is much higher than the value of amorphous Si (≈1 cm^2 V^{-1} s^{-1}).[9] However, things have been changed in 2004, since the first report of high-performance flexible thin-film transistors (TFTs) based on amorphous InGaZnO (a-IGZO), a transparent amorphous oxide semiconductor (TAOS) with electron mobility as high as 10 cm^2 V^{-1} s^{-1}.[9] From then on, TAOS TFTs as well as the fundamental material science have been extensively investigated and now they are being used in commercial large-area flat-panel displays.[10] According to previous researches related with a-IGZO, Ga element is a necessary stabilizer in the amorphous structure since gallium oxide will not crystallize unless the substrate temperature is higher enough, whereas indium oxide and zinc oxide tend to crystallize readily even at room temperature (RT).[11] It indicates amorphous gallium oxide (a-GaO$_x$) could be realized more easily compared with indium oxide and zinc oxide. As a matter of fact, a-GaO$_x$ has also attracted a great deal of attention due to its wide bandgap and high breakdown field strength. At the earlier stage, a-GaO$_x$ thin films were mainly used as a dielectric layer or a passivation layer in microelectronic devices and solar cells.[12,13] In 2017, three groups reported solar-blind UV PDs using a-GaO$_x$ thin films almost simultaneously.[14–16] It is quite interesting that the performance of UV PD using a-GaO$_x$ is comparable or even better than its crystalline counterpart.[15,17] Except for UV PDs, a-GaO$_x$ materials also have extensive applications in areas of solar cells,[18–21] phosphors,[22,23] resistance random access memories (RRAMs),[24–27] gas sensors,[28] and radiation detectors.[29] These versatile applications together with the fact that scalable a-GaO$_x$ can be easily prepared on almost any substrates make it appealing for flexible electronics and giant microelectronics. Great attention has been paid to this cost-effective material, evidenced by the increased number of publications retrieved with the key word of "amorphous Ga$_2$O$_3$," as shown in **Figure 1**.

To further understand the material properties of a-GaO$_x$ and construct superior UV PDs, it is necessary to summarize the progresses on a-GaO$_x$ materials and devices. In this Review, we will

Dr. H. Liang, Z. Han, Prof. Z. Mei
Songshan Lake Materials Laboratory
Dongguan, Guangdong 523808, China
E-mail: hlliang@iphy.ac.cn; zxmei@iphy.ac.cn

Dr. H. Liang, Z. Han, Prof. Z. Mei
Beijing National Laboratory for Condensed Matter Physics
Institute of Physics
Chinese Academy of Sciences
Beijing 100190, China

Z. Han
School of Physical Sciences
University of Chinese Academy of Sciences
Beijing 100049, China

The ORCID identification number(s) for the author(s) of this article can be found under https://doi.org/10.1002/pssa.202000339.

DOI: 10.1002/pssa.202000339

 © 2020 Wiley-VCH GmbH

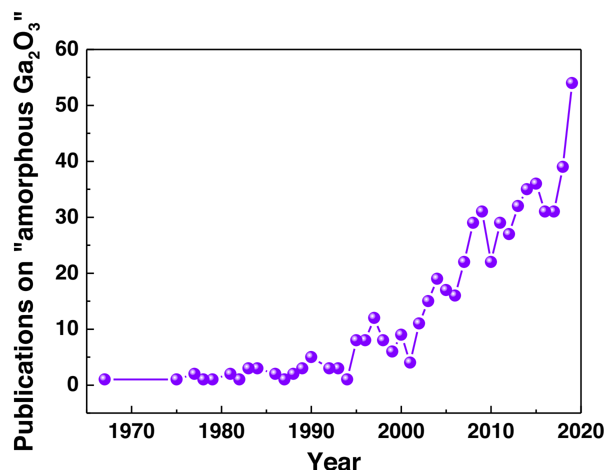

Figure 1. Number of publications related with amorphous Ga_2O_3 from 1967 to the end of 2019 (Data: Web of Science).

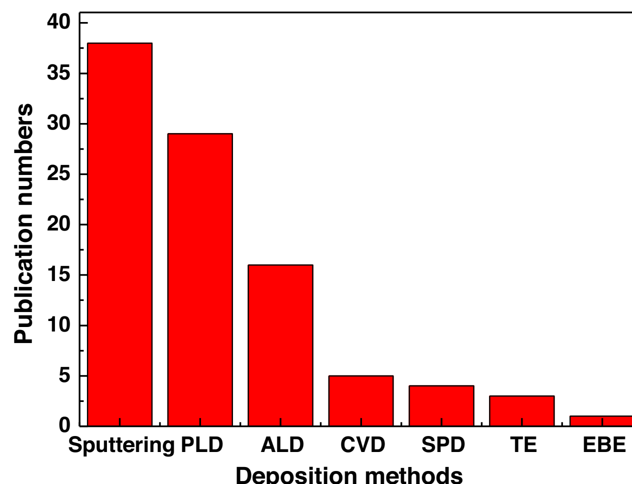

Figure 2. Several representative methods used for the preparation of a-GaO_x in literatures.

first introduce the main-stream preparation methods for a-GaO_x films, primarily focusing on the dependence of stoichiometry, crystallinity, optical, electrical, and morphological properties on growth process. Doping and alloying as well as device studies will be discussed in the second part. These achievements may provide a better understanding on a-GaO_x materials and UV PDs, probably facilitating the promotion of its detection performance and the exploration of its new optoelectronic applications in wide areas.

2. Preparation Methods of a-GaO_x

To prepare amorphous materials, the most important factor is deposition temperature. A proper temperature should be chosen to avoid the crystallization of the materials. As mentioned earlier, crystallization of gallium oxide will happen at high temperatures ($\approx>400\,°C$),[30–37] indicating it is quite easy to synthesize a-GaO_x materials below this temperature. Conventional thin-film deposition methods, including radio-frequency (RF) magnetron sputtering, pulsed laser deposition (PLD), atomic layer deposition (ALD), chemical vapor deposition (CVD), thermal evaporation (TE), electron-beam evaporation (EBE), and solution process deposition (SPD) have been widely explored to synthesize a-GaO_x. The histogram in **Figure 2** is used to graphically summarize the distribution of publications and researchers' preference for these growth techniques. It can be clearly seen that sputtering, PLD and ALD are more preferred, among which sputtering and ALD are well-suited for large-area thin-film deposition in industry, whereas PLD is often used to seek the mechanism behind the materials and devices in laboratory. In next subsections, we will go into more details about the specific parameters of these different strategies for a-GaO_x fabrication.

2.1. RF Sputtering

Sputtering, as a well-developed thin-film deposition technique, has been widely applied to produce thin films in industry with advantages such as simple apparatus, low deposition temperature, high deposition rate, and good adhesion along with uniformity and suitability for large area deposition.[38] As Ga_2O_3 target is usually nonconductive due to its ultralarge bandgap, it can only be prepared using RF source. Saikumar et al. has summarized recent results related with RF-sputtered β-Ga_2O_3 thin films, from which we can see many factors including substrate temperature, working pressure, oxygen partial pressure, RF power can affect the characteristics of the films.[38] Considering the aforementioned factors, a table has been made related with RF-sputtered a-GaO_x materials (**Table 1**), where some typical features can be outlined.

1) Most of the a-GaO_x thin films were deposited on the inexpensive substrates like glass/quartz, polyethylene terephthalate (PET), polyethylene naphthalate (PEN), polyimide (PI); 2) Most of the a-GaO_x thin films were deposited at RT with low energy consumption; 3) The surface morphology is quite smooth with root mean square (RMS) values in the range of 0.55–2.102 nm; 4) Without alloying or doping with other elements, the variation of a-GaO_x bandgap energy is much smaller than the one prepared by PLD as the deposition parameter changes, which will be discussed in next subsection.

In general, the substrate temperature (T_s) is a key parameter in thin-film deposition process. It influences the microstructures and properties of the sputtered films. Several groups have carried out related experiments on the role of T_s. Kumar et al. have produced gallium oxide thin films by varying T_s in a wide range (25–800 °C) and found that lower temperatures result in amorphous structure, whereas $T_s \geq 500\,°C$ leads to nanocrystalline.[32] The morphology changes from the featureless smooth surface to a fine microstructure of dense particles with increased average particle size as T_s increases. The bandgap of the films varies from 4.96 to 5.17 eV for a variation of T_s. The variation of O/Ga ratio as a function of T_s is revealed by Rutherford backscattering spectrometry (RBS) measurements. The results indicate that the O/Ga ratio of films grown at RT is 1.6, slightly higher than 1.5 for the stoichiometric Ga_2O_3. A T_s of 300 °C or higher is

© 2020 Wiley-VCH GmbH

Table 1. Summarization of different processing parameters of RF-sputtered Ga_2O_3 films.

Substrate	T_s [°C]	Power [W]	Gas flow [sccm]	Pressure [Pa]	Thickness [nm]	RMS [nm]	Bandgap [eV]	Application area	Ref.
SiO_2/Si Glass	RT	60	–	–	25	0.55	–	Three terminal UV PD	[39]
Quartz	RT	60	Ar	0.4	150	0.554	–	Ozone sensor	[28]
Quartz	RT-500	80	Ar	2	57.3–93.07	2.16–0.794	4.96–4.79	Solar-blind UV PD	[40]
PEN	RT	60	Ar/O_2 10/–	0.4	250	–	–	Flexible X-ray detector	[29]
Sapphire	RT	80	Ar/40	5	200	≈1	4.2	a-Ga_2O_3:In solar-blind UV PD	[41]
PET	RT	50	Ar/O_2 10/10	1	–	1.55	5.02	3D solar-blind UV PD	[42]
SiO_2/Si	RT	60	Ar/30	0.4	208	1.07	–	Field-effect phototransistor and imaging	[43]
Sapphire	RT	180	Ar/O_2 40/4	0.4	125	–	4.9	Solar-blind UV PD	[44]
SiO_2/Si	RT	–	Ar	2	60	–	4.9	RRAM under UV light	[45]
Sapphire	RT-750	–	Ar/O_2 6:1 mix	1	200	–	4.93–5.05	Solar-blind UV PD	[36]
PI	50–200	120	Ar/20	3.325	200	–	4.8	Flexible solar-blind UV PD	[46]
Quartz PET	RT	100	Ar	0.665	–	–	–	Flexible solar-blind UV PD	[47]
Sapphire	RT	180	Ar/O_2 40/4	1	120 min	–	4.02–5.04	Photodetector	[17]
Quartz	RT	100	Ar/20	0.35–1.2	279–416	–	4.64–4.94	Solar-blind UV PD	[48]
PI	RT	–	Ar/O_2 1:1 mix	0.4	100	–	–	Flexible RRAM	[24]
Sapphire	600	150	Ar/O_2	0.665	120	–	4.56–5.04	Deep UV PD	[49]
PET Glass	RT	–	Ar/O_2	0.665	80–225	<0.6	3.1–4.8	a-CdGaO thin films	[50]
Glass	RT	125	Ar/10	0.399	25 + 100	–	4.06	Copper-doped a-Ga_2O_3	[51]
SiO_2/Si	RT	–	Ar/O_2 10/10	–	4.5	–	–	Memory devices	[52]
Glass	RT	100/40	Ar/O_2 50/0; 49/1; 48/2	–	100	–	4.414; 4.446; 4.464	a-IGO solar-blind UV PD	[53]
Si (100)	25–700	100	Ar	–	200	–	–	Mechanical performance	[54]
Glass	RT	(100/90)/ (40/50/60)	–	–	10 + 40	–	–	a-IGO TFT	[55]
SiO_2 glass	RT	50, 100	Ar/10	2.5	–	–	2.5, 3.0, 3.9	Vacuum annealing effects on a-CdGaO thin films	[56]
Sapphire	450	50	Ar/O_2 65/3	–	100	2.102	4.83	Solar-blind UV detector	[15]
Glass PEN	RT	60	Ar/O_2 10/(0–0.15)	0.4	250	–	5.03	Solar-blind UV PD	[16]
Si (100)	500	100	Ar/O_2	–	200	–	–	Mechanical properties of GaMoO thin films	[57]
ITO glass	≈400	–	Ar/25	0.8	480	–	–	RRAM	[58]
SiO_2 glass	RT	50, 100	Ar/10	2.5	≈100	–	2.5–4.3	a-CdGaO thin films	[59]
Glass	RT	100	Ar/O_2 35/45	–	50	–	3.95–4.4	a-IGO UV phototransistors	[60]

© 2020 Wiley-VCH GmbH

Table 1. Continued.

Substrate	T_s [°C]	Power [W]	Gas flow [sccm]	Pressure [Pa]	Thickness [nm]	RMS [nm]	Bandgap [eV]	Application area	Ref.
Glass	RT	–	Ar/O_2	–	100	–	4.7	a-Ga_2O_3/CIGS visible light detection	[61]
Glass	–	–	Ar/O_2	–	10	–	–	a-IGZO/a-Ga_2O_3 UV phototransistors	[62]
Glass	550	100	Ar/20	0.665	15–1350	–	4.19–5.08	Structural and optical evolution with thickness	[63]
Si	25–600	100	Ar	–	40	0.5–3.0	4.96–5.17	Chemical bonding, optical constants, electrical resistivity	[33]
Glass	RT	–	Ar/O_2 30/30	–	200	–	–	a-Ga_2O_3/SiO_2 dual dielectric	[64]
TiN/SiO_2/Si	–	–	Ar/O_2 30/10	–	30	–	–	a-IGO RRAM	[65]
Si Quartz	25–800	100	Ar	–	40–33	–	4.96–5.17	Structural and optical evolution	[32]
Glass	RT	75	Ar/O_2	0.2	190–200	1.2	3.74–3.94	a-IGO TFT	[66]
Si (100)	RT	25	Ar/O_2 7:3 mix	1.995	550	–	–	Ga_2O_3:Mn, green-emitting phosphor	[67]

required for the formation of stoichiometric Ga_2O_3 films. The authors further studied the chemical bonding, surface morphological characteristics, optical constants, and electrical properties of the sputtered films with T_s from 25 to 600 °C.[33] Wang et al. simply tuned the growth temperature from RT to 750 °C with the formation of amorphous/crystalline gallium oxide phase junctions and realized high-performance solar-blind UV PDs.[36] Zhu et al. demonstrated solar-blind UV PDs based on a-GaO_x thin films prepared at different T_s (RT-500 °C) and found that photodetectors using the 500 °C deposited thin films possessed the best performance.[40] Battu et al. also found that gallium oxide films deposited at T_s = RT-400 °C were amorphous and the amorphous-to-crystalline transformation occurred at T_s = 500 °C.[54] All of the aforementioned results indicate that T_s can greatly affect not only the material properties but also the device performance. Thus, an appropriate T_s should be selected deliberately.

Except substrate temperature, oxygen partial pressure is another key parameter that strongly influences the oxide material and related devices' performance. Cui et al. found that a delicate control of the oxygen flux from 0 to 0.15 sccm during the sputtering process played a key role in affecting the a-Ga_2O_3 solar-blind UV PD performance with a metal–semiconductor–metal (MSM) structure. Both the dark current and photocurrent of these devices decrease as oxygen flux increases, which is attributed to the increase in the Schottky barrier height (SBH) between the ITO electrode and a-Ga_2O_3 thin film.[16] Liang et al. explored the probability of a-Ga_2O_3 as an X-ray detecting material and found a strong dependence of X-ray photocurrent on oxygen partial pressure during the sputtering growth.[29] Zhang et al. reported the conversion of Ti/a-Ga_2O_3 contact from ohmic to Schottky by tuning the conductivity of a-Ga_2O_3 films with the help of a delicate control of oxygen flux during the sputtering process.[44] Kikuchi et al. investigated the electrical and optical properties of a-Ga_2O_3/Cu(In,Ga)Se_2 (CIGS) heterojunction photodiodes where gallium oxide layer is used as a hole-blocking layer and buffer layer. The oxygen partial pressure during Ga_2O_3 deposition was optimized to minimize the dark current.[61] Chang et al. reported the fabrication of a-IGZO/a-GaO_x bilayer phototransistors and found that the phototransistors' performance strongly depended on the oxygen partial pressure during the deposition of the gallium oxide layer.[64] These results reveal the importance of oxygen introduction during the sputtering process and provide an effective strategy to modulate the a-Ga_2O_3 device performance.

2.2. PLD

PLD is another physical vapor deposition technique for the preparation of oxide thin films with advantages of ultrahigh vacuum, high deposition rate, and controllable gas environments (reduction, oxidation, or protection gases). During the pulsed-laser ablation of the Ga_2O_3 target, a plasma plume constituted by gaseous Ga–O species (Ga, O, Ga_2O, and other gallium-oxygen molecules in fundamental or excited states)[26] will deposit onto the substrates, where T_s, oxygen partial pressure and laser power will greatly affect the microstructural, optical, and electrical properties of a-GaO_x films, as shown in **Table 2**. A-GaO_x films obtained by PLD system usually have such characteristics as listed in the following: 1) Most of the a-GaO_x thin films were deposited on rigid substrates like glass, sapphire, and Si, while few results have been reported on flexible plastic substrates so far; 2) The RMS values of these films (3.2–6 nm) are much higher than those achieved via RF sputtering deposition (0.55–2.102 nm); 3) The variation of a-GaO_x bandgap is larger than the one prepared in RF sputtering system as the deposition parameter changes as the Ga/O ratio can be modulated far below the stoichiometric level using PLD technique; 4) Unlike most of

© 2020 Wiley-VCH GmbH

Table 2. Summarization of different processing parameters of PLD-grown a-GaO_x films.

Substrate	T_s [°C]	λ_{Laser} [nm]	Rate [Hz]	E_{Laser} [mJ]	Gas	Pressure [Pa]	Thickness [nm]	RMS [nm]	E_g [eV]	Application area	Ref.
Sapphire	250–650	248	2	300	O_2	1	847.8–720.2	–	4.6–5.1	UV photodetector	[37]
Glass	250	266	10	95 mJ cm^{-2}	O_2	0–6.65	100	–	–	UV photodetector	[68]
Al_2O_3	300	248	10	220	O_2	0.01	320	–	4.31	Broadband photodetector	[48]
Sapphire	400–1000	–	–	700	–	–	332–69	–	4.7–5.0	Optical properties	[35]
Glass	RT	248	10	1.8 J cm^{-2}	O_2	1–25	120	–	4.17–4.26	Inorganic thin-film phosphors	[23]
Glass	RT	248	–	2 J cm^{-2}	O_2	0–20	120	–	–	a-GO:Cr_x thin films for red PL	[22]
Glass	250	266	10	95 mJ cm^{-2}	O_2	0–6.65	100	3.2–4.9	4.45–4.75	Effect of oxygen partial pressure	[69]
Sapphire	450–650	248	1	2.3 J cm^{-2}	Vacuum/Ar/O_2	–	65	–	3.0–5.0	a-$Ga_2(O_{1-x}S_x)_3$	[70]
Alumina	RT	248	10	200	O_2	4	500	6	–	Isotopic oxygen diffusion	[71]
Sapphire	290–500	248	–	225	O_2	0.1	–	–	4.40–5.11	Optical properties and band structure	[34]
Sapphire	200–600	248	2	225	O_2	0.1	–	–	–	Ga_2O_3:Eu films	[72]
Glass	RT	248	–	30–80	O_2	0–10	50, 120, 140	–	0.5–4.12	Insulator-to-semiconductor conversion	[73]
Glass	100	248	10	300	O_2	0.65	5–10	–	–	Diffusion barrier layer in CIGS solar cells	[19]
Al_2O_3	500–700	–	–	–	Vacuum	1×10^{-6}	–	–	4.11–4.82	Vo migration driven by bias	[74]
Quartz	100–425	–	–	–	O_2	2×10^{-3} 0.13	10, 200	–	4.0–4.5	V_O and Sn doping of a-Ga_2O_3	[75]
Glass	260–520	–	–	–	Ar/O_2	0.133	–	–	–	Transparent conducting oxides	[76]
Nb:$SrTiO_3$	500	248	1	400	Vacuum	2×10^{-5}	150	–	–	Memory	[77]
Glass	−25	248	2	200	–	–	–	–	–	Work function of TCOs	[78]
Nb:$SrTiO_3$	500	248	1	400	Vacuum	2×10^{-5}	150	–	–	Memory	[25]
Quartz	400	248	10	300	O_2	1.33×10^{-4}	200	–	–	Dopant activation in a-Ga_2O_3:Sn	[79]
Pt/Ti/SiO_2/Si	500	–	–	–	Vacuum	1×10^{-6}	200	–	–	Memory	[80]
Pt/Ti/SiO_2/Si	300	–	–	–	Vacuum	1×10^{-6}	200	–	–	Memory	[26]
Glass	RT	248	10	300	Ar	3.99	90	–	–	Memory	[27]
Sapphire	400	266	–	(50–200) $\times 10^6$ W/cm^2	O_2	0–0.02	50–400	–	–	Oxygen deficient a-GaO_x	[81]
Cu_2O sheets	RT	193	20	350 mJ cm^{-2}	O_2	0–2.2	20–90	–	–	n-Ga_2O_3/p-Cu_2O solar cell	[82]
Sapphire; SiO_2/Si	RT-500	266	–	–	Vacuum	10^{-5}	≈200	–	–	Phase separation	[31]
Sapphire; Si; NaCl	300–500	266	5	0.5–2 J cm^{-2}	O_2	0–10	50–500	–	1.6–4.9	Metallic clusters	[30]
Glass	450	248	5	1.5 J cm^{-2}	Vacuum O_2	7×10^{-5} 20	–	–	3.62; 4.92	Resistive switching	[83]
Sapphire	500–600	248	–	200	O_2 N_2 Ar	4	1000–6000	<6	1.81–3.61	Insulator-to-metal transition	[84]

© 2020 Wiley-VCH GmbH

the RF-sputtered a-GaO_x thin films worked as photodetectors, most of the PLD deposited a-GaO_x thin films were used as resistive switching memory devices due to the abundant oxygen vacancy (V_O) defects.

Several groups have evaluated the influence of T_s on the properties of a-GaO_x thin films. In the study by Zhang et al.,[34] gallium oxide films were prepared by PLD at oxygen pressure of 0.1 Pa and T_s varied from 290 to 500 °C where amorphous-to-crystalline transition took place above 350 °C. Abrupt bandgap value variation (≈4.4 eV in amorphous state and ≈5.0 eV in crystalline state) was observed and attributed partly to the V_O and extra subgap density of states.[34] Yang et al. also deposited a series of gallium oxide thin films on sapphire substrates with different growth temperatures (400, 550, 700, and 1000 °C) and only the sample grown at 400 °C is amorphous without any detectable X-ray diffraction (XRD) peaks from crystalline gallium oxide. The optical bandgap also shows a blue shift from 4.7 to 5.0 eV as growth temperature increases.[35] Wu et al. fabricated a series of gallium oxide thin films on sapphire substrate via PLD with T_s ranging from 250 to 650 °C and found that the crystallization procedure started at about 450 °C as well as a blue shift presenting at the absorption edge (from 4.6 to 5.1 eV) with T_s increasing from 450 to 650 °C.[37] In the study by Guo et al.,[74] gallium oxide films were deposited on α-Al_2O_3 substrates at various T_s (500, 550, 600, 650, and 700 °C) in a vacuum environment. At low growth temperature (500 °C), the film is XRD amorphous, strong oxygen deficiency, low transparency, and high conductivity. As T_s increases, the energy bandgap increases from 4.11 eV for 500 °C to 4.82 eV for 700 °C. I–V hysteretic loop and current-turning voltage of the amorphous sample is strongly dependent on the voltage-sweep rate, which can be attributed to the migration of V_O defects driven by bias.[74] Heinemann et al. investigated oxygen deficiency and Sn doping in a-GaO_x thin films grown at a temperature gradient from 425 to 300 °C and from 160 to 100 °C with fixed oxygen partial pressure of 2×10^{-5} and 1.3×10^{-3} mbar, respectively.[75] All the films show an amorphous structure for T_s up to 425 °C. The O/Ga ratio decreases significantly and becomes constant around 1.3 at temperatures below 300 °C together with a same decrease trend of the bandgap from 4.5 eV for 425 °C to a constant value around 4.0 eV for T_s below 300 °C, indicating that the substoichiometry, likely as a result of the low-deposition temperature, is the reason for the reduced bandgap. Combined with C–V and J–V curves, it is argued that the origin of this bandgap reduction is the formation of a V_O defect band locating closely to the conduction band minimum (CBM) level. Lim et al. prepared Ga_2O_3:Sn thin films via PLD method with different fabrication temperatures, Sn concentrations, and oxygen partial pressures, and found that the film transparency was obviously affected due to the formation of Ga suboxide phase at low growth temperature without O_2, and regardless of Sn concentration.[76] From the aforementioned discussion, it can be found that T_s plays an important role for the fabrication of Ga oxide thin film, which will strongly influence its crystalline state and optical bandgap.

Except for the crystallization and bandgap modulation related with T_s, an interesting chemically driven insulator–metal transition (conductivity increases from $<10^{-4}$ to 10^3 S cm^{-1}) has been first observed on amorphous $GaO_{1.2}$ thin film (deposited between 773 and 873 K) when heating it up to 673 K in an inert atmosphere by Nagarajan et al.[84] This phenomenon has been attributed to the formation of a Ga_2O_3 nucleus surrounded by a small Ga metallic region. However, Hebert et al. found that the as-deposited oxygen-deficient $Ga_2O_{2.3}$ films grown under vacuum at RT would still remain amorphous, transparent, and insulating even after a postdeposition annealing at 673 K in vacuum (10^{-7} mbar) for 2 h.[31] On the contrary, Ga oxide films grown at a substrate temperature of 673 K at 10^{-7} mbar are optically absorbing, electrically conducting and partly crystalline, indicating the formation of Ga metallic clusters in a stoichiometric matrix in situ at moderate substrate temperatures (673 K) without postdeposition annealing.[31] Further, Petitmangin et al. carried out a more systematic study to explore the properties of a-Ga_2O_x thin films with a wide range of oxygen deficiency and more specifically discuss the case of large deficiency with $x \leq 2.3$.[30] The film was grown at T_s varied between 300–500 °C under the pressure changing from 10^{-7} up to 0.1 mbar via oxygen introduction. Through the investigation of the temperature-dependent resistivity and wavelength-dependent optical constants, together with XRD and transmission electron microscope (TEM) characterization, it is deduced that the largely oxygen-deficient Ga oxide films, due to a disproportionation reaction, are heterogeneous and contain metallic Ga clusters embedded in a stoichiometric or nearly stoichiometric crystalline β-Ga_2O_3 phase. These references demonstrate that the microstructure of Ga oxide thin films can be effectively controlled through substrate temperatures, which will in turn modulate the films' electrical and optical properties.

Oxygen-deficient Ga oxide films are easily obtained with substoichiometry and low transparency via PLD technique. Petitmangin et al. have summarized the average film composition as a function of oxygen pressure and flux of Ga atoms per pulse. From this summarization, all Ga oxide films are oxygen deficient except the one grown at very high oxygen pressure (0.1 mbar).[30] As reported by Nagarajan et al., a pronounced insulator–metal transition was observed for the films prepared in Ar while no conductivity jump was found for the amorphous but stoichiometric gallium oxide prepared in oxygen,[84] indicating the growth atmosphere would greatly affect the physical properties of such Ga oxide thin films. Therefore, it is natural to introduce oxygen gas to modulate the film properties and related device's performance. For example, Minami et al. demonstrated high-efficiency n-Ga_2O_3/p-Cu_2O-based heterojunction solar cells, where n-Ga_2O_3 thin film was fabricated in PLD with oxygen gas pressure varied from 0 to 2.2 Pa. It was found that the best performance was from the device using a 75 nm n-Ga_2O_3 fabricated under oxygen pressure of 1.7 Pa, which may be attributed to a decrease in defect levels at the interface of n-Ga_2O_3/p-Cu_2O.[82] Kim et al. have reported semiconducting a-GaO_x thin films deposited on glass at RT and their applications in TFTs and Schottky diodes. As opposed to the cases of conventional oxide semiconductors and previously reported insulator–metal transition of a-$GaO_{1.2}$ by Nagarajan et al.,[84] an appropriately high oxygen partial pressure must be chosen for a-GaO_x to reduce electron traps. Too low (<1 Pa) or too high (>6 Pa) oxygen partial pressure will produce insulating films. Under the optimized condition, semiconducting a-GaO_x thin films with an electron Hall mobility of ≈8 cm^2 V^{-1} s^{-1}, a carrier density N_e of $\approx 2 \times 10^{14}$ cm^{-3} and an ultrawide bandgap of ≈4.12 eV

© 2020 Wiley-VCH GmbH

have been successfully achieved.[73] Recently, Oanh et al. fabricated a series of Ga oxide thin films on glass substrate at $T_s = 250\,^\circ C$ via PLD with oxygen pressure varied from 0 to 50 mTorr.[85] All of the as-grown thin films are XRD amorphous. The measured RMS roughness values of the as-grown thin films increase from 3.2 to 4.9 nm as oxygen pressure increasing from 0 to 50 mTorr. The calculated optical bandgaps are 4.45, 4.92, 4.83, 4.76, and 4.75 eV when the oxygen partial pressure increases from 0 to 20, 30, 40, and 50 mTorr, respectively. In addition, unlike previous result in the study by Kim et al.,[73] the conductivity of the as-grown thin films reduces monotonically from 7.9 to 2.1 mS cm^{-1} as oxygen pressure increases, which may relate with the different deposition temperatures. Further, they have fabricated a series of UV PDs with MSM structure using the aforementioned Ga oxide thin films and found that both of the photoresponsivity and response speed will increase as oxygen pressure increases,[68] revealing the important role of the oxygen processing gas in promoting device performance.

2.3. ALD

Within the aforementioned deposition techniques, ALD is considered as one of the most promising methods with its inherent and unique advantages such as precise thickness control, excellent step coverage, and high conformality and uniformity for the preparation of ultrathin layers. It is worth to be noted that, in contrast with other growth methods, ALD can provide precise atomic-scale thickness control and much purer films at lower temperatures, which is attributed to the self-saturating and self-limiting characteristics of the ALD process.[86] Compared with a-Ga_2O_3 thin films deposited by RF sputtering or PLD technique, the hallmarks of ALD grown films are briefly summarized: 1) Due to the inherent self-limiting characteristic of ALD deposition process, the growth rate is quite lower than RF sputtering and PLD, providing precise thickness control in atomic-scale level; 2) Most of the deposition temperature windows are below 400 °C, indicating it is suitable for depositing a-Ga_2O_3 thin films; 3) To obtain high-quality Ga_2O_3 thin films, it is important to choose appropriate Ga and oxygen precursors. A variety of researches have been conducted to find out the most practical and applicable couples of Ga and oxygen precursors; 4) Unlike the oxygen-deficient thin films prepared by PLD system, nearly all of the a-Ga_2O_3 thin films obtained through ALD method are stoichiometric with decent electrical and optical properties.

The first successful ALD process for Ga_2O_3 was demonstrated by Nieminen et al. using $Ga(acac)_3$ and either water or ozone, but relatively high deposition temperatures (>370 °C) were required, and an acceptable composition was only obtained with ozone.[87] To date, different Ga and oxygen precursors have been reported for the deposition of Ga_2O_3 thin films in ALD processes, as shown in **Table 3**. The ever-reported Ga precursors include trimethylgallium (TMGa),[14,86,89,90,93,95,98,99] triethylgallium (TEGa),[92] tris (2,2,6,6-tetramethyl-3,5-heptanedionato) gallium(III) ($Ga(TMHD)_3$),[96] and gallium tri-isopropoxide (GTIP).[97] Most of these precursors could only be used at a high temperature (>300 °C) typically resulting in undesired impurities within the films such as carbon and hydrogen, whose concentrations strongly depend on the growth temperature.[89] As TMGa has a high vapor pressure and is highly volatile, it could be used as a gallium source at lower temperatures. However, as previously reported, TMGa with H_2O_2 or H_2O could not grow gallium oxide via ALD, even at a higher deposition temperature of 350 °C because the surface became poisoned by surface methyl species after only a few cycles and these methyl species could not be removed by H_2O.[99] Although Ga_2O_3 alone could not be deposited using TMGa and H_2O_2 as Ga and oxygen precursors, respectively, Gallium could be doped into the oxide film at 200 °C when accompanied by an InO subcycle [(InCA-1)-H_2O_2], as reported by Sheng et al. In doing so, an atomic composition of over 20% Ga could be obtained.[93] In addition to that, more active oxygen precursors such as ozone and oxygen plasma have also been used when TMGa is used as Ga source. For example, in the study by Comstock and Elam,[99] alternating exposures to TMGa and ozone yielded a growth rate of 0.52 Å/cycle for deposition temperatures between 200 and 375 °C. The use of oxygen plasma further lowers down deposition temperature by increasing the chemical reaction rate while decreasing the interlayer diffusion rate, thereby effectively broadening the ALD temperature window.[89] Several groups have reported their results using TMGa and oxygen plasma for Ga_2O_3 deposition with a temperature window between 50 and 400 °C and a growth rate ranging from 0.53 to 0.7 Å per cycle.[86,89,95,98]

Except using TMGa as Ga precursor, some other metal organics containing Ga element have also been developed to synthesize Ga_2O_3 thin films. Choi et al. deposited Ga_2O_3 thin films using GTIP as a gallium source and H_2O as an oxygen source at a low temperature (150–250 °C) in a thermal ALD system.[97] The growth rate is as high as ≈2.5 Å per cycle. The Ga/O ratio was measured as 1:1.7 by RBS. All of the films are amorphous, smooth, and transparent. More importantly, the ALD Ga_2O_3 thin film prepared at 250 °C demonstrates superior electrical properties (leakage current $\approx 1 \times 10^{-11}$ A at 1 MV cm^{-1} and breakdown field ≈7.6 MV cm^{-1}), which is considered to be closely linked with its slightly oxygen-rich nature. Ramachandran et al. have grown a-Ga_2O_3 using $[Ga(TMHD)_3]$ as a gallium source with enhanced volatility and thermal stability.[96] They tested H_2O, O_3, and O_2 plasma and found that only O_2 plasma resulted in successful deposition of gallium oxide. The growth rate is quite lower (0.1 Å per cycle), which may be beneficial for doping process where the concentration of the dopant has to be precisely controlled. O'Donoghue et al. first reported low temperature synthesis of gallium oxide using $[Ga(NMe_2)_3]_2$ and O_2 plasma.[94] This precursor couple yielded a high growth rate of 1.5 Å per cycle due to the high volatility and reactivity nature of both reactive species. The as-deposited layers were homogenous, amorphous, nearly stoichiometric ($Ga/O = 0.61 \pm 0.08$) with an optical bandgap of 4.9 eV. Recently, Mizutani et al. deposited Ga_2O_3 thin films using liquid compound pentamethylcyclopentadienyl gallium (GaCp*) as gallium source as this material has a relatively high vapor pressure and thermal stability up to 250 °C.[88] The obtained Ga_2O_3 film was a high-purity thin film having a stoichiometric composition ($O/Ga = 1.5$) and almost no C impurity, indicating that GaCp* is a promising candidate precursor for forming high-quality Ga_2O_3 films.

© 2020 Wiley-VCH GmbH

Table 3. Summarization of different processing parameters of ALD-grown a-Ga_2O_3 films.

Substrate	T_s [°C]	Ga precursor	Pulse time [s]	T_{Ga} [°C]	O precursor	Pulse time [s]	GR [Å/cycle]	Composition	Bandgap [eV]	Ref.
Si	200	GaCp*	0.1–0.3	80	H_2O, O_2 plasma	1–5/40–90;	0.6	O/Ga = 1.5	–	[88]
Si	80–200	TMGa	0.01	–	O_2 plasma	5	0.7–0.63	Ga/O = 2/3 (T_S = 150)	4.63 ± 0.05	[89]
Si	200	TMGa	0.02	13	O_2 plasma	5	0.7 (pure Ga_2O_3)	Ga/O = 0.63 (pure Ga_2O_3)	4.64–5.25	[90]
		DEZn	0.2	20	H_2O	0.2				
Si	80–250	TMGa	0.5	13	O_2 plasma	10	0.7	Ga/O = 0.71	4.6–4.8	[86]
Quartz										
Quartz	105–195	DMA_4Sn, $((CH_3)_2N)_4Sn$; DMA_3Ga, $((CH_3)_2N)_3Ga$	1	40 (Sn) 80 (Ga)	H_2O	1	0.6–0.8	O/Me = 1.7	2.7–4.2	[91]
4H-SiC	250	TEGa	0.03	–	H_2O	0.03	–	–	6.0	[92]
		CP_2Mg								
Si/SiO_2	120	Bis-tetrakis-digallium	3 Torr s	107	H_2O	5 Torr s	–	–	–	[20]
Si	200	InCA-1	1	40	H_2O_2	0.5	0.42	–	–	[93]
		TMGa	0.2	–						
Si	60–160	$[Ga(NMe_2)_3]_2$	0.5 × 4	110	O_2 plasma	2	1.5	Ga/O = 0.63 ± 0.08	4.9	[94]
Glass	≈<250	TMGa	1.5	5	Ozone	5	–	Ga/O = 0.58	4.8	[14]
PI										
Si/SiO_2	120	Bis-tetrakis-digallium; Tetrakis-tin	3 Torr s; 2 Torr s	120; 60	H_2O	5 Torr s	2	$Ga_2O_{3.41}$ $Sn_{0.065}$	–	[79]
Si	50–150	TMGa	–	–	O_2 plasma	–	0.7	–	4.6	[95]
Si/SiO_2	100–400	Ga $(TMHD)_3$	5	135	O_2 plasma	5	0.1	Ga/O = 0.64	4.95	[96]
Si, glass, carbon	150–250	GTIP	–	120	H_2O	–	2.5	Ga/O = 1/1.7	5.4	[97]
Si	100–400	TMGa	0.015	6	O_2 plasma	20	0.53	Ga/O = 0.69	–	[98]
Si; fused SiO_2	200–350	TMGa	0.5	–	Ozone	3	0.52	Ga/O = 2/3	4.95	[99]

2.4. Other Methods

Even though CVD technique can provide high-quality layers with practical growth rates and excellent control of purity, uniformity, and composition, publications of CVD grown a-Ga_2O_3 are quite few. As early as in 2004, Kim et al. prepared large-scale gallium oxide nanowire arrays on sapphire substrates using a reaction of a TMGa and oxygen mixture at a temperature of 600 °C by metal organic chemical vapor deposition (MOCVD) method.[100] No XRD patterns of the gallium oxide were observed, revealing that the nanowires are fully amorphous. Zhao et al. deposited Sn-doped Ga_2O_3 thin film on n^+-Si substrate using trimethylgallium, tetraethyltin, and pure oxygen as precursors by MOCVD at a substrate temperature of 400 °C.[101] The Sn:Ga_2O_3 film showed an amorphous-like structure with the Sn dopant mainly in Sn^{4+} oxidation state, which acted as a shallow donor in Ga_2O_3. Takiguchi et al. investigated low temperature deposition of gallium oxide-related films by MOCVD at a temperature below 272 °C using TMGa and H_2O.[102] The deposition at T_s of 92 °C did not show any films on the substrate. A flat film consisting of several gallium oxide-related phases was grown at T_s of 182 °C. A nanowire film was grown at T_s of 272 °C. These films had small amount carbon and hydrogen contaminants because this growth temperature was not high enough to decompose TMGa. These contaminations could be removed by postdeposition annealing at 300 °C in ambient air. In the study by Kobayashi et al.,[21] hydrogenated a-GaO_x thin films were grown using plasma-enhanced chemical vapor deposition (PECVD) at temperatures below 200 °C with high deposition rates, achieving high broadband transparency, wide bandgap (3.5–4 eV), and low refractive index (1.6 at 500 nm).[21] The potential of these films as a second antireflective coating layer in Si heterojunction solar cells was also demonstrated. Zhang et al. first deposited Mg:GaO_x (MGO) film on n-Si wafers via MOCVD method under 700 °C, where dicyclopentadienyl magnesium (CP2Mg) and TEGa were adopted as the precursors.[103] Except for the characteristic XRD peaks related to silicon substrate, no other diffraction peaks related with the MGO film were observed, manifesting that the prepared film was amorphous. The optical bandgap was estimated as 5.1 eV. Solar-blind UV PDs were fabricated using MGO films. Compared with undoped a-GaO_x UV PD, the MGO-based UV PD exhibited a lower dark current of 48 pA, a larger on/off ratio ($I_{255\ nm}/I_{dark}$) of 338, and a faster response speed (a rise time of 0.02 s and a decay time of 0.15 s). Its low dark current and fast response speed can be attributed to the reduction of oxygen vacancies induced by the Mg divalent ions doping in the a-GaO_x film.

© 2020 Wiley-VCH GmbH

Vacuum thermal evaporation is one of the simplest and inexpensive deposition techniques that is suitable for fabricating high-quality films. However, there are only a few studies on Ga_2O_3 thin films prepared by vacuum thermal evaporation from Ga_2O_3 powders.[104–106] In the study by Shi et al.,[104] gallium oxide thin films were deposited on quartz substrates at RT by thermal evaporation of Ga_2O_3 powder placed on a tungsten crucible. Base vapor pressure in the evaporator was about 3×10^{-4} Pa and the heating current was 200 A.[104] These thin films annealed at lower temperatures were amorphous, whereas those annealed at above 800 °C were nanocrystalline. The annealing temperature increasing from 400 to 1100 °C results in the bandgap increase from 4.70 to 5.13 eV due to the reduction in density of defect states. As reported by Kalygina et al., the thermal-evaporated gallium oxide thin films are inhomogeneous with regions of enhanced and decreased thickness, respectively.[105] Rao and Kumar deposited a-GaO_x thin films by resistively heating Ga_2O_3 powder in a Mo-boat or a Ta-boat at ambient substrate temperature with vacuum of $\approx 3 \times 10^{-4}$ Pa.[106] The pristine films are oxygen deficient (Ga/O = 1.3), amorphous, and absorbing in UV–vis region. Except for thermal evaporation, electron beam evaporation (EBE) is also an efficient and convenient technique for thin-film deposition with low cost and high deposition rate. Cheng et al. conducted Cu-doped Ga_2O_3 thin films by EBE where a high voltage of 6 kV was applied to the source.[107] The substrate was heated at 400 °C. The as-grown sample shows gradual absorption, indicating that the sample is amorphous and lacks a distinct absorption edge.

In addition to the vacuum deposition, chemical solution deposition in atmosphere has also been adopted to synthesize a-GaO_x thin films due to its low cost. For instance, Cabello et al. developed a photochemical metal organic deposition method to prepare films of gallium oxide doped or codoped with Tb, Eu, Mn, and Cr. Solutions of the inorganic complexes were spin coated on substrates and photolyzed at RT using 254 nm UV light. The resulting films are nonstoichiometric with amorphous structure.[108,109] Xiang et al. used the spin-coating method to form gallium oxide films on p-type silicon substrate as a surface passivation layer, where gallium nitrate solution was used. An amorphous-to-crystalline phase transformation happened as the annealing temperature was increased above 550 °C.[18] Chen et al. reported the fabrication of gallium oxide thin films by a novel polymer-assisted deposition method with a facile single-step spin-coating process, which had an accurate control of thickness, homogeneity, stoichiometry, and interface roughness.[110] The 500 °C-annealed GaO_x film using this process exhibited smooth surface, amorphous nature, and excellent dielectric performance.

3. UV PDs using a-GaO_x Thin Films

Benefiting from the various and facile deposition methods of a-GaO_x, a variety of UV PDs have been reported. In the following section, we will comprehensively review recent advances in a-GaO_x-based UV PDs including their basic parameters of photoresponsivity, response speed, and detectivity. Corresponding working mechanisms and physics will also be discussed.

MSM structure with simple interdigital finger electrodes is the most common architecture to construct photodetectors, where two back-to-back Schottky junctions form, as shown in **Figure 3**a,b from Qian et al.[15] In their work, superior responsivity and recovery time have been demonstrated on RF-sputtered a-GaO_x thin films, which are even better than the MBE-deposited β-Ga_2O_3 thin film, as shown in Figure 3c,d. The a-GaO_x PD has a high responsivity of 70.26 A/W, much higher than that of the β-Ga_2O_3 PD (4.21 A/W). The better performance is attributed to the existence of large internal gain and sub-bandgap transitions.

Later, Lee et al. also showed the great potential of a-Ga_2O_3 as deep UV PDs with MSM structure (**Figure 4**a).[14] Ultrathin (3–50 nm) a-GaO_x films were grown on glass or PI substrates by low-temperature (≈<250 °C) ALD technique. Devices using the 30 nm-thick GaO_x films work reliably only in deep UV spectrum region with a maximum responsivity of 45.11 A/W at $\lambda = 253$ nm (Figure 4b). The dark current measured at 10 V is as low as 200 pA and the signal-to-noise ratio reaches up to $\approx 10^4$ (Figure 4c). In addition, the rise time (i.e., the time interval for photocurrent to increase from 10% to 90%) is as short as 2.97 μs at $\lambda = 266$ nm (Figure 4d). This ALD-grown a-GaO_x films herein provide an economically viable and cost-effective solution for the development of diverse deep UV photodetector applications.

In the same year of 2017, Cui et al. conducted a comprehensive study of the effect of tuning oxygen flux in a mild way on a-Ga_2O_3 solar-blind-photodetectors' response speed for the first time.[16] a-Ga_2O_3 films were deposited by RF-magnetron sputtering at RT with oxygen flux of 0, 0.12, 0.13, 0.14, and 0.15 sccm, respectively. All of the thin films were transparent with no obvious bandgap shift, as shown in **Figure 5**a. As oxygen flux increased, both of the dark current and photocurrent decreased significantly (Figure 5b,c), which was ascribed to the increased SBH. Robust improvement in the response speed was achieved by subtly varying the oxygen flux. The device exhibited an ultrafast decay time of 19.1 μs and a responsivity of 0.19 A/W (shown in Figure 5d,f). The promotion of temporal response speed was mainly due to the reduction of V_O concentration in the film deposited with higher oxygen flux. This approach also worked in flexible a-Ga_2O_3 UV PDs. No obvious degradation of the device performance was observed in bending states and fatigue tests, providing a cogent demonstration of flexible solar-blind UV PDs based on sputtered a-Ga_2O_3 thin films.

In 2019, Jiao et al. deposited a-Ga_2O_3 thin films at RT and annealed these films at 500, 600, 700, 800, and 900 °C in air ambiance.[17] MSM PDs with Au electrodes were constructed with these as-grown and annealed thin films, respectively. Compared with the apparently more than two orders of magnitude UV response of the as-grown a-Ga_2O_3 thin film, the polycrystalline β-Ga_2O_3 films after annealed at high temperatures show photocurrents under 254 nm light in the same level as the dark current (**Figure 6**), indicating that a-Ga_2O_3 thin film has potential applications for solar-blind UV photodetection.

Taking the advantage of low-temperature growth, Chen et al. realized an a-Ga_2O_3 3D solar-blind PD array via an origami route, as shown in **Figure 7** with a number of unique properties such as extremely wide detection space angle and excellent spatial

© 2020 Wiley-VCH GmbH

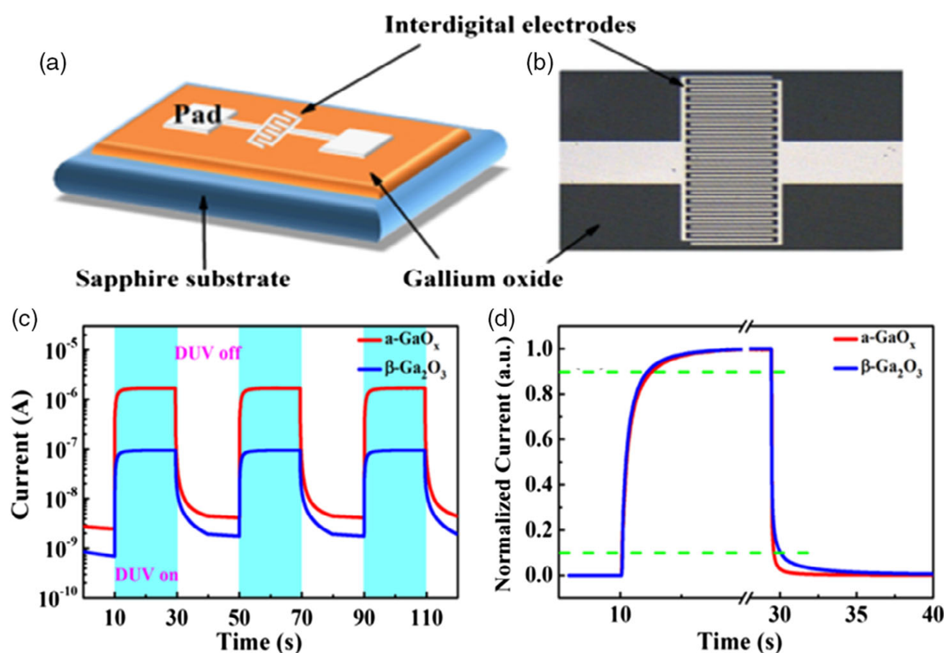

Figure 3. a) Schematic diagram and b) photograph of a typical gallium-oxide MSM PD fabricated on a *c*-plane sapphire substrate. c) Transient response of the MSM PDs based on a-GaO_x and β-Ga_2O_3 thin films for multicycles on a semilogarithmic scale. d) Normalized response on a linear scale. Reproduced with permission.[15] Copyright 2017, American Chemical Society.

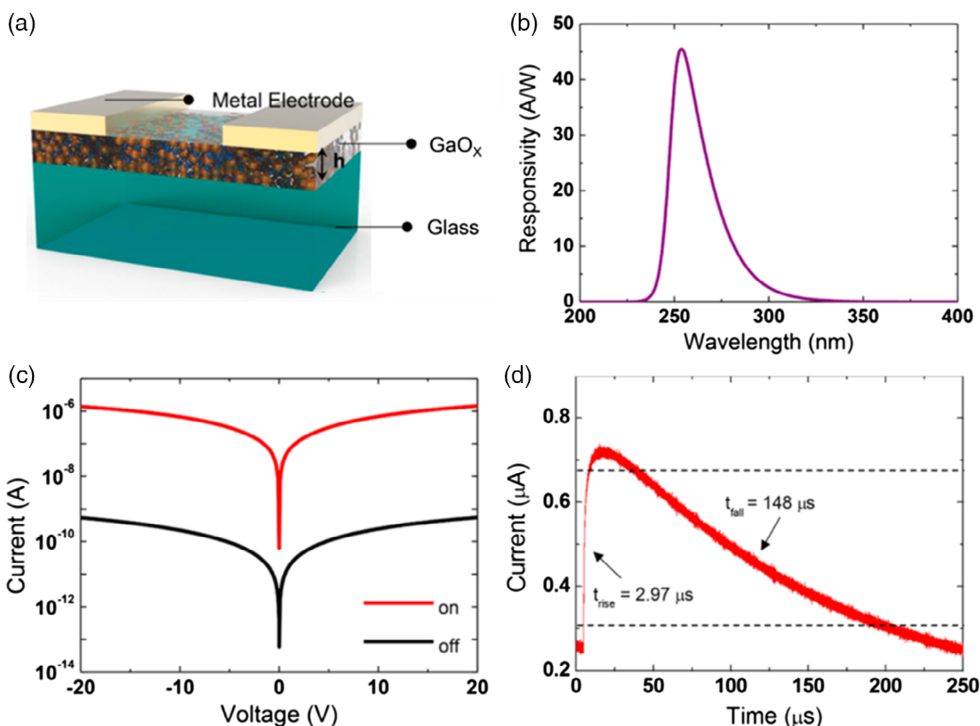

Figure 4. a) Schematic of the fabricated MSM-type photodetector. b) Responsivity as a function of wavelength of illuminated light at 20 V. c) Current–voltage curve of the photodetector depending on deep UV illumination. d) Photocurrent as a function of the time to measure the rise time of the photodetector using a 30 nm-thick a-GaO_x thin film. Reproduced with permission.[14] Copyright 2017, American Chemical Society.

recognition.[42] The a-Ga_2O_3 films were grown on PET substrates. The photodetector exhibited a relatively high spectral selectivity for solar-blind UV light detection with UV/visible rejection ratio over 10^3 and solar-blind ratio over 10^2. The maximum

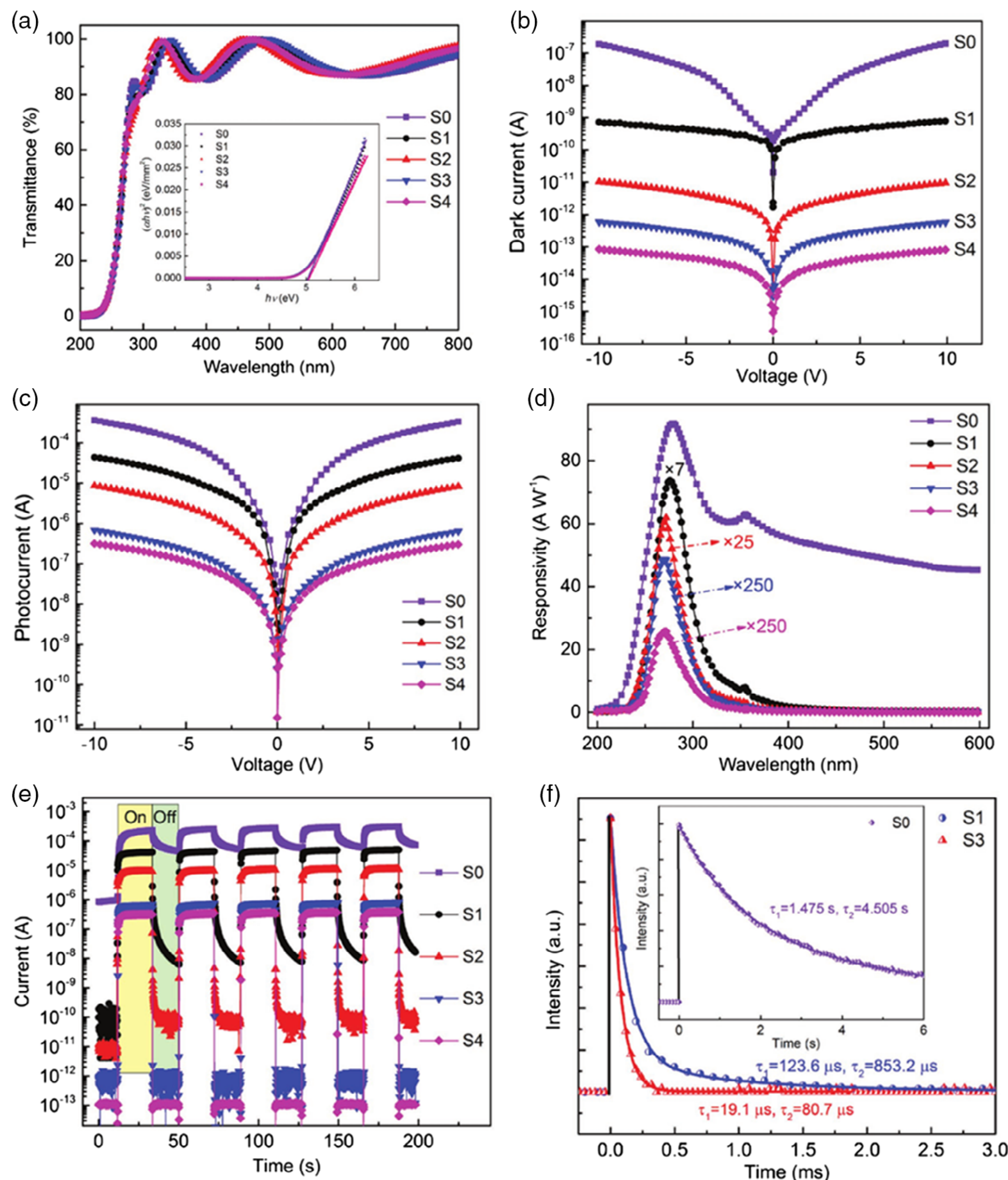

Figure 5. a) The optical transmittance spectra of the a-Ga_2O_3 films. The inset shows the plot of $(\alpha h\nu)^2$ versus $h\nu$ for a-Ga_2O_3 films. b) *I*–*V* curves in dark and c) under UV 254 nm light illumination. d) Photoresponsivity spectra of the PDs biased at 20 V. e) Time-dependent photoresponse of S0–S4 with the UV 254 nm light on and off at 10 V bias. f) Temporal response tests of the PDs with KrF pulse laser illumination at 10 V bias. Reproduced with permission.[16] Copyright 2017, Wiley-VCH.

responsivity was 8.9 A/W at 250 nm with a low dark current of 0.17 nA under 15 V bias. The photodetector cells revealed excellent electrical stability after thousands of bending cycles due to the unique nature of amorphous structure of the Ga_2O_3 films.

Except for the application as deep UV PDs, a broad-spectrum photodetector based on a-Ga_2O_3 film was exhibited by Zhou et al.[48] Using the subgap absorption related to V_O detects, the devices exhibited high responsivity over a wide spectral range from deep UV to near infrared (NIR) (250–875 nm). The responsivity at 250, 350, 525, and 850 nm was as high as 1099, 265, 205, and 122 A/W, respectively. What's more, the persistent photocurrent (PPC) effect commonly accompanied with abundant V_O defects could be effectively eliminated by a short-time heating, which made the response recovery time significantly decrease from hours to seconds. With no need of doping or alloying, a-Ga_2O_3 UV–NIR broadband photodetector with high gain and fast recovery speed opens up new possibilities for future high-performance photodetections.

As a decent UV PD, high responsivity and fast response speed have always been pursued. Many efforts have been devoted to realize such devices either by optimizing film deposition processes or by designing different device structures. In the following, we will discuss how the device performance can be improved from both of the material and device viewpoints.

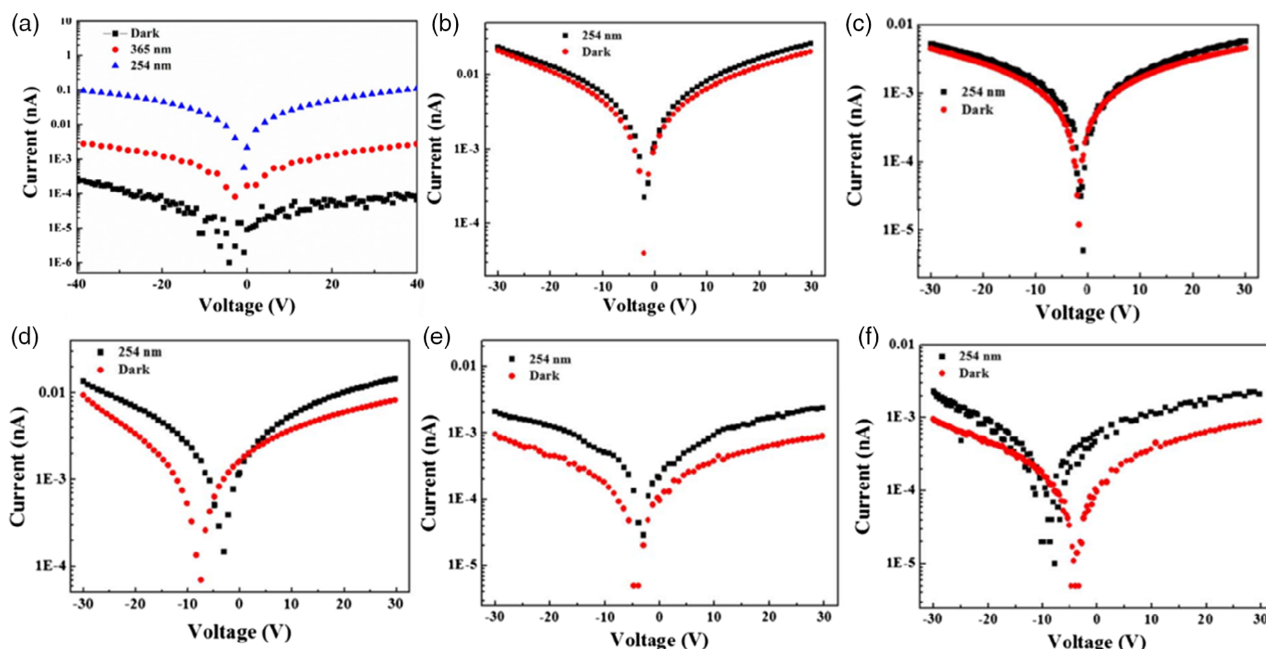

Figure 6. a) Current–voltage characteristic of the MSM junction made from as-grown amorphous film in dark and with 365, 254 nm illumination. Current–voltage characteristic of the MSM junction made from annealed film in dark and with 254 nm illumination, annealing temperature is b) 500 °C; c) 600 °C; d) 700 °C; e) 800 °C; and f) 900 °C. Reproduced under the terms of the Creative Commons Attribution 4.0 license.[17] Copyright 2019, The Authors, published by Electrochemical Society.

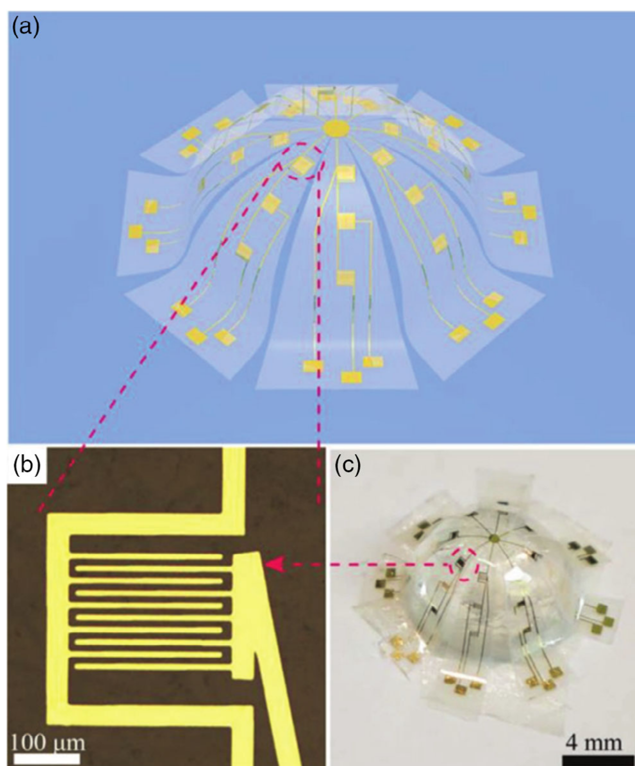

Figure 7. a) Schematic of the 3D a-Ga_2O_3 photodetector array. b) Microscope image of an individual photodetector cell. c) Photograph of the 3D a-Ga_2O_3 photodetector array. Reproduced with permission.[42] Copyright 2019, Wiley-VCH.

As discussed in the study by Cui et al.,[16] intrinsic V_O defects in a-Ga_2O_3 film play a critical role in determining the UV PDs' performance. Zhang et al. demonstrated a conversion behavior from ohmic to Schottky contacts at Ti/Ga_2O_3 interface by regulating the conductivity of a-Ga_2O_3 films with delicate control of oxygen flux in the RF-sputtering process.[44] For a-Ga_2O_3 film deposited without oxygen, abundant donor-like V_O defects near the metal-Ga_2O_3 interface facilitated the tunneling process across the barrier, resulting in the contact conversion from Schottky to ohmic, which elevated the photocurrent and dark current simultaneously but degraded the light-to-dark ratio. On the contrary, Vu et al. showed a different result with a-Ga_2O_3 film grown by PLD at 250 °C with a modulation of various oxygen partial pressures from 0 to 50 mTorr during the deposition process.[68] All of the films were XRD amorphous, as shown in **Figure 8**. Unlike the result using RF-sputtered a-Ga_2O_3 where both of the dark current and photocurrent decreased but photoresponse speed increased as more and more oxygen flux was introduced into the growth chamber in the study by Cui et al.,[16] the dark current of the PDs using PLD-grown a-Ga_2O_3 did not change while both photoresponsivity and response speed increased concurrently when oxygen partial pressure increased, as shown in Figure 8b–d. Therefore, the highest photoresponsivity of 5 A/W and fastest decay time of 33 ms were obtained at the highest oxygen partial pressure of 50 mTorr under 254 nm UV illumination. This phenomenon was attributed to the reduction of oxygen vacancies caused by the increase in oxygen content during deposition, revealing the importance of the oxygen processing gas in promoting photodetector performance.

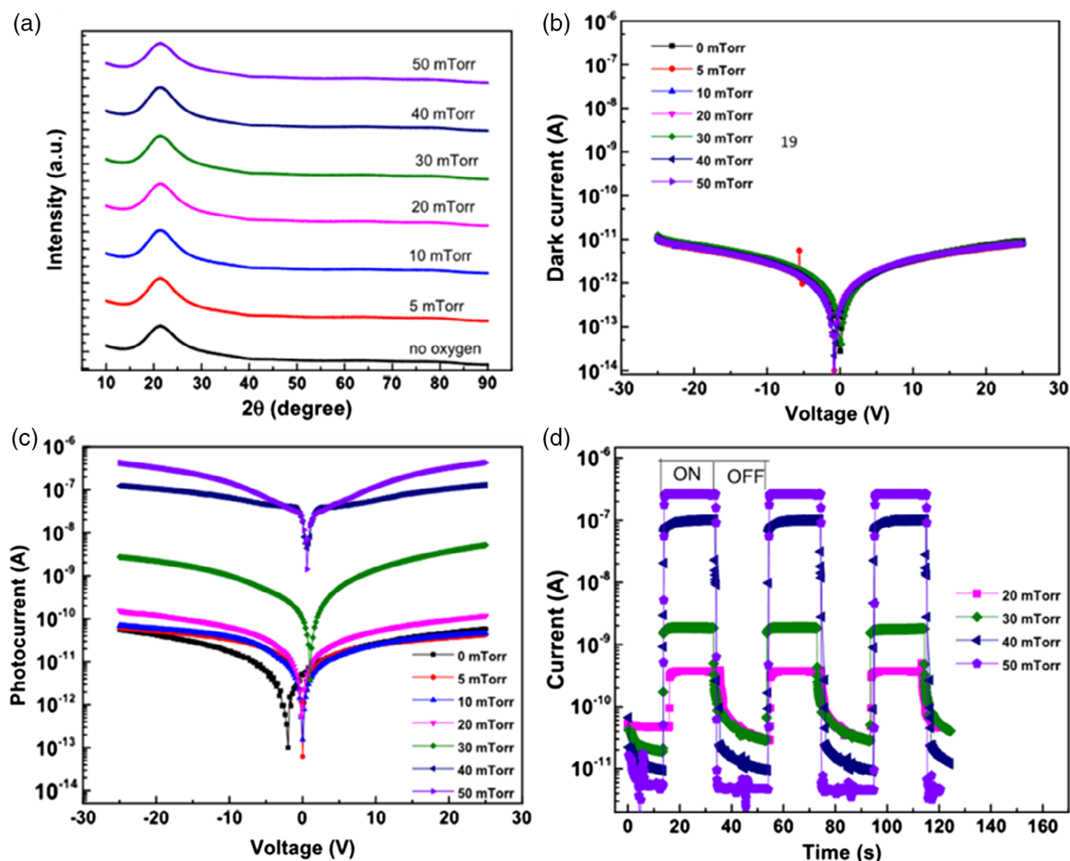

Figure 8. a) XRD patterns of as-grown Ga_2O_3 films grown on glass under various oxygen pressures. b) Dark *I–V* curves and c) photocurrent–voltage curves under illumination of 254 nm for devices fabricated under various oxygen pressure. d) Repetitive photoresponse of Ga_2O_3 PDs under the different oxygen pressure from 20 to 50 mTorr. Reproduced with permission.[68] Copyright 2020, IOP Publishing Ltd.

Han et al. conducted the modulation of Ar pressure during a-Ga_2O_3 film fabrication by RF-magnetron sputtering and developed a high-performance UV PD.[111] The device with maximum responsivity of 436.3 A/W (under 240 nm UV light) was obtained on the film deposited at 0.5 Pa, which is mainly due to the quasi-Zener tunneling multiplication mechanism between different resistance areas in a-Ga_2O_3 thin films.

In addition to the gas atmosphere, tuning deposition temperature during the fabrication of a-Ga_2O_3 thin films is also a crucial method to optimize the performance of UV PDs. For example, Li et al. demonstrated a process of tuning temperatures (50–200 °C) during the Ga_2O_3 film fabrication by RF-magnetron sputtering, where the Ga_2O_3 film remained amorphous structure.[46] At the highest temperature of 200 °C, the devices exhibited the best performance with responsivity of 52.6 A/W under 254 nm UV light illumination and the photo-to-dark current ratio of more than 10^5. Interestingly, Wang et al. fabricated Ga_2O_3 film by RF-magnetron sputtering with one step at a specific temperature range, where the film maintained a transitional state composing of both amorphous and crystalline phases.[36] The coexistence of amorphous and crystalline phases was formed between 400 and 500 °C, below which the film was purely amorphous and above which the film was purely crystalline. PDs with MSM structure were fabricated using films grown at different temperatures. From **Figure 9**a, all photodetectors exhibit similarly small dark

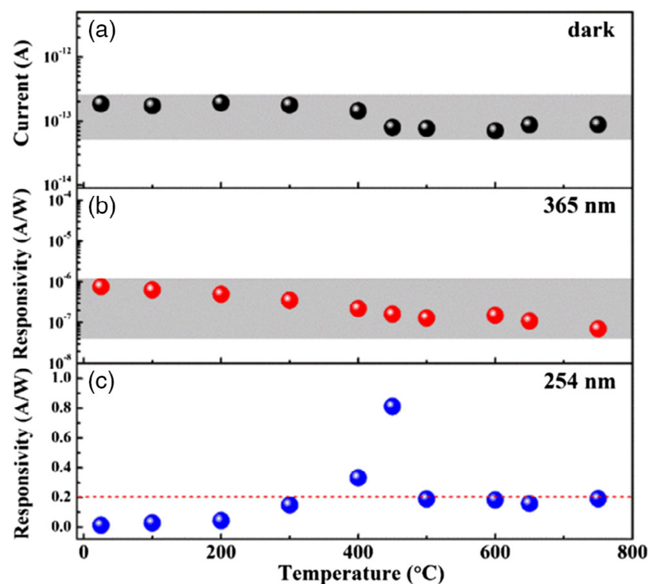

Figure 9. a) Dark current as a function of substrate temperature without UV illumination at RT. b,c) Responsivity as a function of temperature under 254 and 365 nm light illumination at 5 V. Reproduced with permission.[36] Copyright 2019, American Chemical Society.

current (≈10^{-13} A at 5 V), independently of the growth temperature, which is of vital importance to enhance the detectivity for the devices. A sharp increase in the photocurrent under 254 nm light illumination is achieved compared with the dark current at the substrate temperature of 450 °C (Figure 9c), which is resulted from the peculiar amorphous/crystalline Ga_2O_3 phase junction. The phase-junction photodetector exhibits a responsivity of 0.81 A/W, a superior detectivity over 5.67×10^{14} Jones, an ultrahigh light-to-dark current ratio over 10^7, and an ultrafast response speed of ≈12 ns/19.6 μs for the rise/decay time.

In addition to the adjustment of the deposition process parameters such as atmosphere and temperature, bandgap engineering of a-Ga_2O_3 with other elements is also an effective strategy to modulate PDs' performance. Among various researches, In and Mg were the two most frequently used elements. Chen et al. studied the amorphous indium–gallium oxide (IGO) MSM-structured solar-blind PDs by cosputtering method, during which three different oxygen concentrations were applied.[53] For the highest oxygen concentration, the a-IGO-based solar-blind PD had an UV-to-visible rejection of 1.1×10^5 and decay time less than 1 s. Fang et al. synthesized the a-IGO alloy with a single sputtering target (Ga:In = 5:2 at%).[41] Based on this a-IGO thin film, the MSM-structured deep UV PDs showed a high responsivity of 18.06 A/W, a fast rise time of 4.9 μs, and decay time of 230 μs under 235 nm UV light illumination. The high responsivity and fast response behaviors were attributed to a quasi-Zener tunneling effect caused by an uneven In distribution in the film. Mg-doped amorphous gallium oxide (a-MGO) film has also been studied as another route to expand the detection range of a-Ga_2O_3-based PDs. Zhang et al. fabricated a-MGO solar-blind UV PDs for the first time.[103] The a-MGO film was deposited on n-Si substrate by MOCVD method at 700 °C. XRD pattern revealed that the MGO film was amorphous even at such a high growth temperature. Compared with the undoped a-Ga_2O_3 deep UV PD, the a-MGO deep UV PD exhibited a lower dark current (48 pA), higher light-to-dark current ratio (≈338 at −3 V bias voltage), and faster response speed (a decay time of 0.15 s). These low dark current and fast response speed were attributed to the reduction of V_O defects induced by Mg doping in a-Ga_2O_3 film. Using a nonequilibrium growth method of plasma-enhanced ALD (PEALD), Dong et al. synthesized an MGO alloy with ultrawide bandgap of 6.0 eV, which could be used to develop vacuum ultraviolet (VUV, $\lambda \leq 200$ nm) PDs (**Figure 10**a).[92] VUV PDs with vertical p-graphene/a-MGO/n-SiC p-i-n structure were constructed and exhibited a typical rectification characteristic (Figure 10b), suggesting it could work in the photovoltaic mode. As shown in Figure 10c,d, the device generated an electric potential difference of 1.72 V under 185 nm illumination and showed a light-to-dark ratio up to 10^3 at 0 V bias. Attributed to the photovoltaic structure, a photoresponsivity of ≈10.3 mA W^{-1} at 0 V bias and a fast response and recovery time of 1.94 μs and 0.6 ms were achieved. The results confirm that a-MGO films have great application potential in VUV detection.

In addition to the aforementioned MSM-structured PDs with two terminals, phototransistors with one more terminal gate to flexibly control the channel carriers' transportation behavior, were considered as an alternative solution to improve PDs' performance. Qin et al. demonstrated a solar-blind field-effect

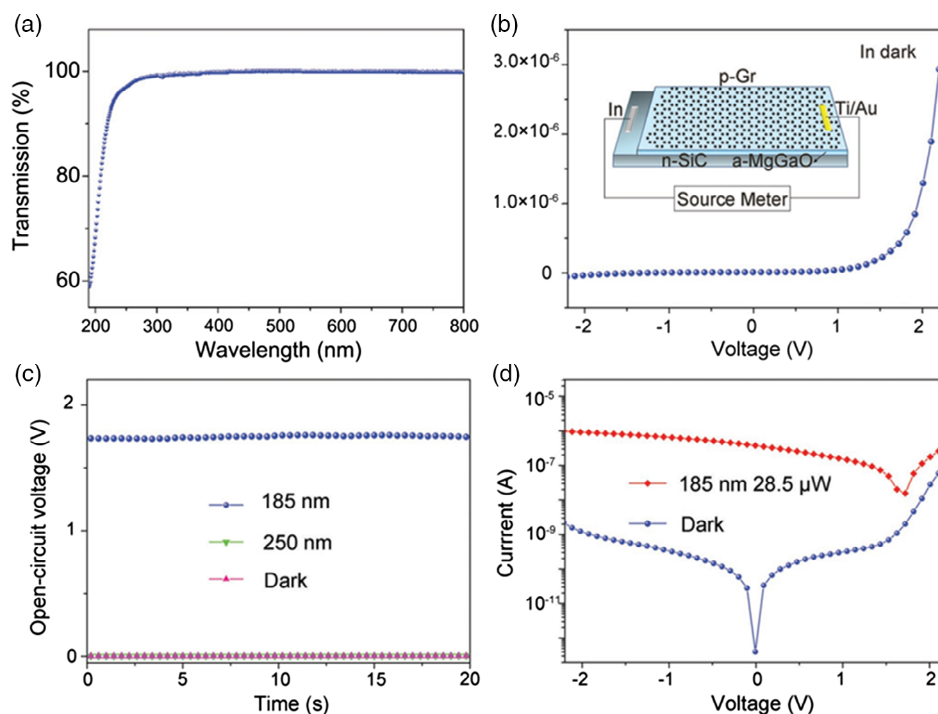

Figure 10. a) Transmission spectrum of a-MGO film on sapphire substrate. b) *I–V* characteristic of single-layer p-graphene/a-MGO/n-SiC detector in dark state. c) Under 0 V bias, the currents of photovoltaic photodetector under dark state, 185 and 250 nm monochromatic light. d) *I–V* characteristics of the p-graphene/a-MGO/n-SiC VUV detector under dark-field conditions and 185 nm monochromatic light (28.5 μW) illumination. Reproduced with permission.[92] Copyright 2019, Wiley-VCH.

phototransistor based on RF-magnetron sputtered a-Ga_2O_3 thin film with ultrahigh photodetection performance.[43] The devices were fabricated on Si substrate with 300 nm SiO_2 as gate dielectric. Due to the high internal gain and field effect control of the phototransistor, the device had ultrahigh responsivity of 4.1×10^3 A/W, external quantum efficiency of 2×10^6%, and detectivity of 2.5×10^{13} Jones under a weak signal of 254 nm UV light with intensity of 70 μW cm^{-2}. The ultrahigh performance indicated significant progress toward the practical application of a-Ga_2O_3 solar-blind UV PDs. Later, Han et al. designed deep UV phototransistors using interdigital drain/source electrodes, as shown in **Figure 11**a, where chemical etching of the RF-magnetron sputtered a-Ga_2O_3 thin film using TMAH solution was first performed before metal deposition.[39] The adoption of the chemical etching of a-Ga_2O_3 channel layer resulted in individual device cells, which lowered the probability of the electrons to transport through the inherent trap sites inside the dielectric layer and facilitated an ultralow dark current of $\approx 10^{-12}$ A (Figure 11b). The devices fabricated on quartz substrate with 100 nm Al_2O_3 as gate dielectric exhibited an excellent n-type TFT performance with an on/off ratio as high as $\approx 10^7$, a high light-to-dark ratio of 5×10^7, a high responsivity of 5.67×10^3 A/W, and a high detectivity of 1.87×10^{15} Jones. Remarkably, the PPC phenomenon was effectively suppressed by applying a positive gate pulse (Figure 11d), which greatly shortened the decay time to 5 ms and offered a-Ga_2O_3 possible roadways into imaging applications.

For a better comparison, some critical parameters related with representative a-GaO_x and crystalline β-Ga_2O_3 UV PDs are shown in **Table 4**. As a common sense, the optoelectronic properties of amorphous materials are quite poor due to the lack of long-range order. However, it can be obviously found that the device performance using crystalline thin films or even bulk crystalline materials does not show the expected overwhelming superiority. By contrast, the performance of amorphous devices is far beyond expectation with high photoresponsivity and fast response speed. Such a distinction together with the fact that a-GaO_x thin films can be easily deposited in a large area makes this material as a promising candidate for deep UV photodetection. Further research should be carried out to dig out this material more deeply.

4. Conclusions

In summary, the recent progresses on a-GaO_x materials and UV PDs have been reviewed. Due to the easy amorphization of gallium oxide material, a-Ga_2O_3 thin films can be readily synthesized at the substrate temperature below 400 °C using the common thin-film deposition technique such as RF-magnetron sputtering, PLD, and ALD. Many parameters including substrate temperature, gas atmosphere, laser power, Ga precursors, and oxygen precursors will greatly affect the stoichiometry, crystallinity, optical, electrical, and morphological properties of the prepared thin films. The influence of substrate temperature and gas atmosphere in sputtering and PLD processes has been thoroughly discussed. As to ALD process, different Ga and oxygen precursors for a-Ga_2O_3 synthesis have been compared. A-GaO_x thin films with a large variation of Ga/O ratio even containing metallic Ga clusters can be obtained using PLD technique, whereas ALD-grown Ga_2O_3 thin films tend to be stoichiometric. Despite such differences, various deep UV

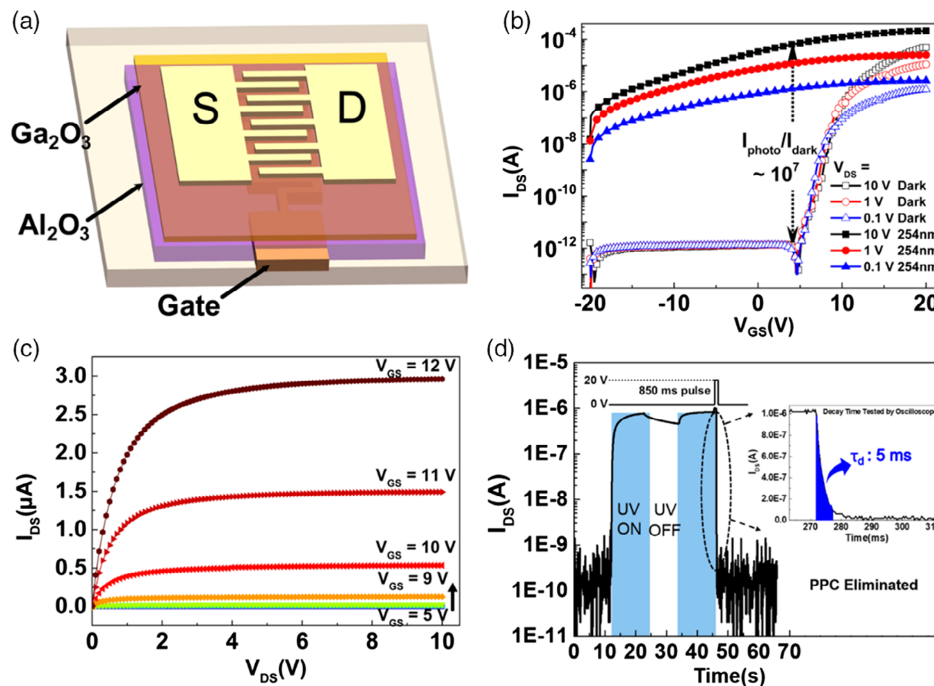

Figure 11. a) Schematic structure of the a-Ga_2O_3 phototransistor on quartz. b) I_{DS}–V_{GS} curves recorded at different V_{DS} in dark and under UV 254 nm light illumination (45 μW cm^{-2}). c) I_{DS}–V_{DS} curves recorded at different V_{GS}. d) Suppression of the PPC with a positive gate pulse. Reproduced with permission.[39] Copyright 2020, Wiley-VCH.

Table 4. Comparison of the main parameters for the reported a-GaO_x and β-Ga_2O_3 photodetectors.

Materials and structures	Methods	*R* [A/W]	*D** [Jones]	Decay time [ms]	Rise time [ms]	Ref.
a-Ga_2O_3 MSM	ALD	45.11	–	–	0.003	[14]
a-GaO_x MSM	Sputtering	70.26	1.26×10^{14}	20	410	[15]
a-Ga_2O_3 MSM	Sputtering	0.19	–	0.019	–	[16]
a-Ga_2O_3 MSM	Sputtering	0.81	5.67×10^{14}	0.0196	1.2×10^{-5}	[36]
a-Ga_2O_3 phototransistor	Sputtering	5.67×10^{3}	1.87×10^{15}	5	–	[39]
a-IGO MSM	Sputtering	18.06	–	0.23	0.0049	[41]
a-GaO_x phototransistor	Sputtering	4.1×10^{3}	2.5×10^{13}	$>4 \times 10^{5}$	5×10^{4}	[43]
a-Ga_2O_3 MSM	PLD	5	1.76×10^{12}	33	100	[68]
a-MGO p-i-n junction	PEALD	0.0103	–	0.6	0.00194	[92]
Bulk β-Ga_2O_3 MSM	EFG*	0.05	–	240	450	[112]
β-Ga_2O_3 MSM	LMBE*	–	–	1020	860	[113]
β-Ga_2O_3 MSM	MOCVD	46	–	800	4500	[114]
β-Ga_2O_3 MSM	Sputtering	96.13	–	78	32	[115]

EFG*: edge-defined film-fed growth; LMBE*: laser molecular beam epitaxy.

PDs using a-GaO_x thin films prepared by different deposition methods have been reported with decent performance, which is comparable with or even better than crystalline Ga_2O_3 counterparts. Thus, considering the facile fabrication process and excellent UV detection performance, the cost-effective a-GaO_x thin films are very appealing for the development of flexible and scalable deep UV PDs in varieties of areas.

Acknowledgements

This work was supported by the National Natural Science Foundation of China (Grant Nos. 11675280, 11674405, 61874139, 11875088, and 61904201) and Guangdong Basic and Applied Basic Research Foundation (2019B1515120057).

Conflict of Interest

The authors declare no conflict of interest.

Keywords

amorphous gallium oxide, flexible electronics, thin films, ultraviolet photodetectors

Received: May 31, 2020
Revised: September 15, 2020
Published online:

[1] D. Walker, M. Razeghi, *Optoelectron. Rev.* **2000**, *8*, 25.
[2] Y. Kokubun, K. Miura, F. Endo, S. Nakagomi, *Appl. Phys. Lett.* **2007**, *90*, 031912.
[3] B. Zhao, F. Wang, H. Chen, L. Zheng, L. Su, D. Zhao, X. Fang, *Adv. Funct. Mater.* **2017**, *27*, 1700264.
[4] S. J. Pearton, J. Yang, P. H. Cary, F. Ren, J. Kim, M. J. Tadjer, M. A. Mastro, *Appl. Phys. Rev.* **2018**, *5*, 011301.
[5] J. Xu, W. Zheng, F. Huang, *J. Mater. Chem. C* **2019**, *7*, 8753.
[6] X. Chen, F.-F. Ren, J. Ye, S. Gu, *Semicond. Sci. Technol.* **2020**, *35*, 023001.
[7] Y. Qin, S. Long, H. Dong, Q. He, G. Jian, Y. Zhang, X. Hou, P. Tan, Z. Zhang, H. Lv, Q. Liu, M. Liu, *Chin. Phys. B* **2019**, *28*, 018501.
[8] X. Chen, F. Ren, S. Gu, J. Ye, *Photonics Res.* **2019**, *7*, 381.
[9] K. Nomura, H. Ohta, A. Takagi, T. Kamiya, M. Hirano, H. Hosono, *Nature* **2004**, *432*, 488.
[10] T. Kamiya, K. Nomura, H. Hosono, *Sci. Technol. Adv. Mater.* **2010**, *11*, 044305.
[11] T. Kamiya, H. Hosono, *NPG Asia Mater.* **2010**, *2*, 15.
[12] T. Hariu, S. Sasaki, H. Adachi, Y. Shibata, *Jpn. J. Appl. Phys.* **1977**, *16*, 841.
[13] M. Passlack, E. F. Schubert, W. S. Hobson, M. Hong, N. Moriya, S. N. G. Chu, K. Konstadinidis, J. P. Mannaerts, M. L. Schnoes, G. J. Zydzik, *J. Appl. Phys.* **1995**, *77*, 686.
[14] S. H. Lee, S. B. Kim, Y.-J. Moon, S. M. Kim, H. J. Jung, M. S. Seo, K. M. Lee, S.-K. Kim, S. W. Lee, *ACS Photonics* **2017**, *4*, 2937.
[15] L.-X. Qian, Z.-H. Wu, Y.-Y. Zhang, P. T. Lai, X.-Z. Liu, Y.-R. Li, *ACS Photonics* **2017**, *4*, 2203.
[16] S. Cui, Z. Mei, Y. Zhang, H. Liang, X. Du, *Adv. Opt. Mater.* **2017**, *5*, 1700454.
[17] S. Jiao, H. Lu, X. Wang, Y. Nie, D. Wang, S. Gao, J. Wang, *ECS J. Solid State Sci. Technol.* **2019**, *8*, Q3086.
[18] Y. Xiang, C. Zhou, W. Wang, *J. Alloys Compd.* **2017**, *699*, 1192.
[19] M. D. Heinemann, M. F. A. M. van Hest, M. Contreras, J. D. Perkins, A. Zakutayev, C. A. Kaufmann, T. Unold, D. S. Ginley, J. J. Berry, *Phys. Status Solidi A* **2017**, *214*, 1600870.
[20] D. Chua, S. B. Kim, R. Gordon, *AIP Adv.* **2019**, *9*, 055203.
[21] E. Kobayashi, M. Boccard, Q. Jeangros, N. Rodkey, D. Vresilovic, A. Hessler-Wyser, M. Döbeli, D. Franta, S. De Wolf, M. Morales-Masis, C. Ballif, *J. Vac. Sci. Technol. Vac. Surf. Films* **2018**, *36*, 021518.
[22] K. Ide, Y. Futakado, N. Watanabe, J. Kim, T. Katase, H. Hiramatsu, H. Hosono, T. Kamiya, *Phys. Status Solidi A* **2019**, *216*, 1800198.
[23] N. Watanabe, K. Ide, J. Kim, T. Katase, H. Hiramatsu, H. Hosono, T. Kamiya, *Phys. Status Solidi A* **2019**, *216*, 1700833.
[24] K.-J. Gan, P.-T. Liu, T.-C. Chien, D.-B. Ruan, S. M. Sze, *Sci. Rep.* **2019**, *9*, 14141.
[25] P. C. Wang, P. G. Li, Y. S. Zhi, D. Y. Guo, A. Q. Pan, J. M. Zhan, H. Liu, J. Q. Shen, W. H. Tang, *Appl. Phys. Lett.* **2015**, *107*, 262110.
[26] D. Y. Guo, Z. P. Wu, Y. H. An, P. G. Li, P. C. Wang, X. L. Chu, X. C. Guo, Y. S. Zhi, M. Lei, L. H. Li, W. H. Tang, *Appl. Phys. Lett.* **2015**, *106*, 042105.
[27] Y. Aoki, C. Wiemann, V. Feyer, H.-S. Kim, C. M. Schneider, H. Ill-Yoo, M. Martin, *Nat. Commun.* **2014**, *5*, 3473.

© 2020 Wiley-VCH GmbH

[28] Y. Sui, H. Liang, Q. Chen, W. Huo, X. Du, Z. Mei, *ACS Appl. Mater. Interfaces* **2020**, *12*, 8929.
[29] H. Liang, S. Cui, R. Su, P. Guan, Y. He, L. Yang, L. Chen, Y. Zhang, Z. Mei, X. Du, *ACS Photonics* **2019**, *6*, 351.
[30] A. Petitmangin, C. Hébert, J. Perrière, B. Gallas, L. Binet, P. Barboux, P. Vermaut, *J. Appl. Phys.* **2011**, *109*, 013711.
[31] C. Hebert, A. Petitmangin, J. Perrière, E. Millon, A. Petit, L. Binet, P. Barboux, *Mater. Chem. Phys.* **2012**, *133*, 135.
[32] S. S. Kumar, E. J. Rubio, M. Noor-A-Alam, G. Martinez, S. Manandhar, V. Shutthanandan, S. Thevuthasan, C. V. Ramana, *J. Phys. Chem. C* **2013**, *117*, 4194.
[33] C. Ramana, V. E. J. Rubio, C. D. Barraza, A. Miranda Gallardo, S. McPeak, S. Kotru, J. T. Grant, *J. Appl. Phys.* **2014**, *115*, 043508.
[34] F. Zhang, H. Li, Y.-T. Cui, G.-L. Li, Q. Guo, *AIP Adv.* **2018**, *8*, 045112.
[35] H. Yang, Y. Liu, X. Luo, Y. Li, D.-S. Wuu, K. He, Z. C. Feng, *Superlattices Microstruct.* **2019**, *131*, 21.
[36] Y. Wang, W. Cui, J. Yu, Y. Zhi, H. Li, Z.-Y. Hu, X. Sang, E. Guo, W. Tang, Z. Wu, *ACS Appl. Mater. Interfaces* **2019**, *11*, 45922.
[37] J. Wu, C. Li, X. Rong, P. Cao, S. Han, Y. Zeng, W. Liu, D. Zhu, Y. Lu, *J. Electron. Mater.* **2020**.
[38] A. K. Saikumar, S. D. Nehate, K. B. Sundaram, *ECS J. Solid State Sci. Technol.* **2019**, *8*, Q3064.
[39] Z. Han, H. Liang, W. Huo, X. Zhu, X. Du, Z. Mei, *Adv. Opt. Mater.* **2020**, *8*, 1901833.
[40] W. Zhu, L. Xiong, J. Si, Z. Hu, X. Gao, L. Long, T. Li, R. Wan, L. Zhang, L. Wang, *Semicond. Sci. Technol.* **2020**, *35*, 055037.
[41] M. Fang, W. Zhao, F. Li, D. Zhu, S. Han, W. Xu, W. Liu, P. Cao, M. Fang, Y. Lu, *Sensors* **2020**, *20*, 129.
[42] Y. Chen, Y. Lu, M. Liao, Y. Tian, Q. Liu, C. Gao, X. Yang, C. Shan, *Adv. Funct. Mater.* **2019**, *29*, 1906040.
[43] Y. Qin, S. Long, Q. He, H. Dong, G. Jian, Y. Zhang, X. Hou, P. Tan, Z. Zhang, Y. Lu, C. Shan, J. Wang, W. Hu, H. Lv, Q. Liu, M. Liu, *Adv. Electron. Mater.* **2019**, *5*, 1900389.
[44] Y.-F. Zhang, X.-H. Chen, Y. Xu, F.-F. Ren, S.-L. Gu, R. Zhang, Y.-D. Zheng, J.-D. Ye, *Chin. Phys. B* **2019**, *28*, 028501.
[45] L. Zhang, H. Yu, L. Xiong, W. Zhu, L. Wang, *J. Mater. Sci. Mater. Electron.* **2019**, *30*, 8629.
[46] Z. Li, Y. Xu, J. Zhang, Y. Cheng, D. Chen, Q. Feng, S. Xu, Y. Zhang, J. Zhang, Y. Hao, C. Zhang, *IEEE Photonics J.* **2019**, *11*, 1.
[47] N. Kumar, K. Arora, M. Kumar, *J. Phys. Appl. Phys.* **2019**, *52*, 335103.
[48] H. Zhou, L. Cong, J. Ma, B. Li, M. Chen, H. Xu, Y. Liu, *J. Mater. Chem. C* **2019**, *7*, 13149.
[49] P.-W. Chen, S.-Y. Huang, C.-C. Wang, S.-H. Yuan, D.-S. Wuu, *J. Alloys Compd.* **2019**, *791*, 1213.
[50] C. P. Liu, C. Y. Ho, R. dos Reis, Y. Foo, P. F. Guo, J. A. Zapien, W. Walukiewicz, K. M. Yu, *ACS Appl. Mater. Interfaces* **2018**, *10*, 7239.
[51] L. Juárez-Amador, I. M. Galván-Arellano, J. A. Andraca-Adame, G. Romero-Paredes, A. Kennedy-Magos, R. Peña-Sierra, *J. Mater. Sci. Mater. Electron.* **2018**, *29*, 15726.
[52] K.-J. Gan, P.-T. Liu, Y.-C. Chiu, D.-B. Ruan, T.-C. Chien, S. M. Sze, *Surf. Coat. Technol.* **2018**, *354*, 169.
[53] K.-Y. Chen, C.-C. Hsu, H.-C. Yu, Y.-M. Peng, C.-C. Yang, Y.-K. Su, *IEEE Trans. Electron Devices* **2018**, *65*, 1817.
[54] A. K. Battu, C. V. Ramana, *Adv. Eng. Mater.* **2018**, *20*, 1701033.
[55] C. P. Yang, S. J. Chang, T. H. Chang, C. Y. Wei, Y. M. Juan, C. J. Chiu, W. Y. Weng, *IEEE Electron Device Lett.* **2017**, *38*, 572.
[56] C. Sato, Y. Kimura, H. Yanagi, *Thin Solid Films* **2017**, *624*, 29.
[57] A. K. Battu, S. Manandhar, C. V. Ramana, *Adv. Mater. Interfaces* **2017**, *4*, 1700378.
[58] Y. S. Zhi, P. G. Li, P. C. Wang, D. Y. Guo, Y. H. An, Z. P. Wu, X. L. Chu, J. Q. Shen, W. H. Tang, C. R. Li, *AIP Adv.* **2016**, *6*, 015215.
[59] H. Yanagi, C. Sato, Y. Kimura, I. Suzuki, T. Omata, T. Kamiya, H. Hosono, *Appl. Phys. Lett.* **2015**, *106*, 082106.
[60] T.-H. Chang, S.-J. Chang, C. J. Chiu, C.-Y. Wei, Y.-M. Juan, W.-Y. Weng, *IEEE Photonics Technol. Lett.* **2015**, *27*, 915.
[61] K. Kikuchi, S. Imura, K. Miyakawa, H. Ohtake, M. Kubota, E. Ohta, *Sens. Actuators Phys.* **2015**, *224*, 24.
[62] S.-J. Chang, T. H. Chang, W. Y. Weng, C. J. Chiu, S. P. Chang, *IEEE J. Sel. Top. Quantum Electron.* **2014**, *20*, 125.
[63] K. H. Choi, H. C. Kang, *Mater. Lett.* **2014**, *123*, 160.
[64] T. H. Chang, C. J. Chiu, S. J. Chang, T. H. Yang, S. L. Wu, W. Y. Weng, *ECS Solid State Lett.* **2014**, *3*, Q55.
[65] J.-B. Yang, T.-C. Chang, J.-J. Huang, Y.-T. Chen, P.-C. Yang, H.-C. Tseng, A.-K. Chu, S. M. Sze, M.-J. Tsai, *Thin Solid Films* **2013**, *528*, 26.
[66] G. Gonçalves, P. Barquinha, L. Pereira, N. Franco, E. Alves, R. Martins, E. Fortunato, *Electrochem. Solid State Lett.* **2010**, *13*, H20.
[67] J. H. Kim, K. H. Yoon, *J. Mater. Sci. Mater. Electron.* **2009**, *20*, 879.
[68] T. K. O. Vu, D. U. Lee, E. K. Kim, *Nanotechnology* **2020**, *31*, 245201.
[69] T. K. Oanh Vu, D. U. Lee, E. K. Kim, *J. Alloys Compd.* **2019**, *806*, 874.
[70] M. Jaquez, P. Specht, K. M. Yu, W. Walukiewicz, O. D. Dubon, *J. Appl. Phys.* **2019**, *126*, 105708.
[71] A. von der Heiden, M. Bornhöfft, J. Mayer, M. Martin, *Phys. Chem. Chem. Phys.* **2019**, *21*, 4268.
[72] K. Nishihagi, Z. Chen, K. Saito, T. Tanaka, Q. Guo, *Mater. Res. Bull.* **2017**, *94*, 170.
[73] J. Kim, T. Sekiya, N. Miyokawa, N. Watanabe, K. Kimoto, K. Ide, Y. Toda, S. Ueda, N. Ohashi, H. Hiramatsu, H. Hosono, T. Kamiya, *NPG Asia Mater.* **2017**, *9*, e359.
[74] D. Y. Guo, Y. P. Qian, Y. L. Su, H. Z. Shi, P. G. Li, J. T. Wu, S. L. Wang, C. Cui, W. H. Tang, *AIP Adv.* **2017**, *7*, 065312.
[75] M. D. Heinemann, J. Berry, G. Teeter, T. Unold, D. Ginley, *Appl. Phys. Lett.* **2016**, *108*, 022107.
[76] K. Lim, L. T. Schelhas, S. C. Siah, R. E. Brandt, A. Zakutayev, S. Lany, B. Gorman, C. J. Sun, D. Ginley, T. Buonassisi, M. F. Toney, *Appl. Phys. Lett.* **2016**, *109*, 141909.
[77] P. G. Li, Y. S. Zhi, P. C. Wang, Z. B. Sun, L. H. Li, Y. H. An, D. Y. Guo, W. H. Tang, J. H. Xiao, *Appl. Phys. A* **2016**, *122*, 663.
[78] T. C. Yeh, Q. Zhu, D. B. Buchholz, A. B. Martinson, R. P. H. Chang, T. O. Mason, *Appl. Surf. Sci.* **2015**, *330*, 405.
[79] S. C. Siah, R. E. Brandt, K. Lim, L. T. Schelhas, R. Jaramillo, M. D. Heinemann, D. Chua, J. Wright, J. D. Perkins, C. U. Segre, R. G. Gordon, M. F. Toney, T. Buonassisi, *Appl. Phys. Lett.* **2015**, *107*, 252103.
[80] D. Y. Guo, Z. P. Wu, L. J. Zhang, T. Yang, Q. R. Hu, M. Lei, P. G. Li, L. H. Li, W. H. Tang, *Appl. Phys. Lett.* **2015**, *107*, 032104.
[81] A. Petitmangin, B. Gallas, C. Hebert, J. Perrière, L. Binet, P. Barboux, X. Portier, *Appl. Surf. Sci.* **2013**, *278*, 153.
[82] T. Minami, Y. Nishi, T. Miyata, *Appl. Phys. Express* **2013**, *6*, 044101.
[83] X. Gao, Y. Xia, J. Ji, H. Xu, Y. Su, H. Li, C. Yang, H. Guo, J. Yin, Z. Liu, *Appl. Phys. Lett.* **2010**, *97*, 193501.
[84] L. Nagarajan, R. A. De Souza, D. Samuelis, I. Valov, A. Börger, J. Janek, K.-D. Becker, P. C. Schmidt, M. Martin, *Nat. Mater.* **2008**, *7*, 391.
[85] V. Oanh, U. L. Dong, K. K. Eun, *J. Alloys Compd.* **2019**, *806*, 874e880.
[86] X. Li, H.-L. Lu, H.-P. Ma, J.-G. Yang, J.-X. Chen, W. Huang, Q. Guo, J.-J. Feng, D. W. Zhang, *Curr. Appl. Phys.* **2019**, *19*, 72.
[87] M. Nieminen, L. Niinistö, E. Rauhala, *J. Mater. Chem.* **1996**, *6*, 27.
[88] F. Mizutani, S. Higashi, M. Inoue, T. Nabatame, *J. Vac. Sci. Technol. A* **2020**, *38*, 022412.
[89] A. Mahmoodinezhad, C. Janowitz, F. Naumann, P. Plate, H. Gargouri, K. Henkel, D. Schmeißer, J. I. Flege, *J. Vac. Sci. Technol. A* **2020**, *38*, 022404.
[90] J. Tao, H.-L. Lu, Y. Gu, H.-P. Ma, X. Li, J.-X. Chen, W.-J. Liu, H. Zhang, J.-J. Feng, *Appl. Surf. Sci.* **2019**, *476*, 733.

© 2020 Wiley-VCH GmbH

[91] F. Larsson, J. Keller, D. Primetzhofer, L. Riekehr, M. Edoff, T. Törndahl, *J. Vac. Sci. Technol. A* **2019**, *37*, 030906.
[92] M. Dong, W. Zheng, C. Xu, R. Lin, D. Zhang, Z. Zhang, F. Huang, *Adv. Opt. Mater.* **2019**, *7*, 1801272.
[93] J. Sheng, E. J. Park, B. Shong, J.-S. Park, *ACS Appl. Mater. Interfaces* **2017**, *9*, 23934.
[94] R. O'Donoghue, J. Rechmann, M. Aghaee, D. Rogalla, H.-W. Becker, M. Creatore, A. D. Wieck, A. Devi, *Dalton Trans.* **2017**, *46*, 16551.
[95] T. G. Allen, A. Cuevas, *Phys. Status Solidi RRL* **2015**, *9*, 220.
[96] R. K. Ramachandran, J. Dendooven, J. Botterman, S. Pulinthanathu Sree, D. Poelman, J. A. Martens, H. Poelman, C. Detavernier, *J. Mater. Chem. A* **2014**, *2*, 19232.
[97] D. Choi, K.-B. Chung, J.-S. Park, *Thin Solid Films* **2013**, *546*, 31.
[98] I. Donmez, C. Ozgit-Akgun, N. Biyikli, *J. Vac. Sci. Technol. Vac. Surf. Films* **2013**, *31*, 01A110.
[99] D. J. Comstock, J. W. Elam, *Chem. Mater.* **2012**, *24*, 4011.
[100] N. H. Kim, H. W. Kim, C. Seoul, C. Lee, *Mater. Sci. Eng. B* **2004**, *111*, 131.
[101] J. L. Zhao, X. W. Sun, H. Ryu, S. T. Tan, *IEEE Trans. Electron Devices* **2011**, *58*, 1447.
[102] Y. Takiguchi, S. Miyajima, *J. Cryst. Growth* **2017**, *468*, 129.
[103] D. Zhang, Z. Du, M. Ma, W. Zheng, S. Liu, F. Huang, *Vacuum* **2019**, *159*, 204.
[104] Q. Shi, Q. Wang, D. Zhang, Q. Wang, S. Li, W. Wang, Q. Fan, J. Zhang, *J. Lumin.* **2019**, *206*, 53.
[105] V. M. Kalygina, V. V. Vishnikina, A. N. Zarubin, V. A. Novikov, Yu. S. Petrova, O. P. Tolbanov, A.V. Tyazhev, S. Y. Tcupiy, T. M. Yaskevich, *Semiconductors* **2013**, *47*, 1130.
[106] P. Rao, S. Kumar, *Superlattices Microstruct.* **2014**, *70*, 117.
[107] Y. Cheng, H. Liang, Y. Liu, X. Xia, R. Shen, S. Song, Y. Wu, G. Du, *Mater. Sci. Semicond. Process.* **2013**, *16*, 1303.
[108] G. Cabello, L. Lillo, C. Caro, M. A. Soto-Arriaza, B. Chornik, G. E. Buono-Core, *Ceram. Int.* **2013**, *39*, 2443.
[109] G. Cabello, A. Araneda, L. Lillo, C. Caro, C. Venegas, M. Tejos, B. Chornik, *Solid State Sci.* **2014**, *27*, 24.
[110] L. Chen, W. Xu, W. Liu, S. Han, P. Cao, M. Fang, D. Zhu, Y. Lu, *ACS Appl. Mater. Interfaces* **2019**, *11*, 29078.
[111] S. Han, X. Huang, M. Fang, W. Zhao, S. Xu, D. Zhu, W. Xu, M. Fang, W. Liu, P. Cao, Y. Lu, *J. Mater. Chem. C* **2019**, *7*, 11834.
[112] F. Qian, H. Lu, H. Genquan, L. Fuguo, L. Xiang, F. Liwei, X. Xiangyu, Z. Jincheng, M. Wenxiang, J. Zhitai, *IEEE T. Electron. Dev.* **2016**, *63*, 3578.
[113] D. Guo, Z. Wu, P. Li, Y. An, H. Liu, X. Guo, H. Yan, G. Wang, C. Sun, L. Li, W. Tang, *Opt. Mater. Express* **2014**, *4*, 1067.
[114] F. Alema, B. Hertog, O. Ledyaev, D. Volovik, G. Thoma, R. Miller, A. Osinsky, P. Mukhopadhyay, S. Bakhshi, H. Ali, W. V. Schoenfeld, *Phys. Status Solidi A* **2017**, *214*, 1600688.
[115] K. Arora, N. Goel, M. Kumar, M. Kumar, *ACS Photonics* **2018**, *5*, 2391.

Huili Liang received her B.S. degree in physics from Beijing Normal University, in 2007, and Ph.D. degree in condensed matter physics from Institute of Physics, Chinese Academy of Sciences (IOPCAS), in 2012. Afterward, she had been working in Renewable Energy Laboratory (REL), IOPCAS. Since 2019, she has been an assistant professor at Songshan Lake Materials Laboratory (SSLAB). Her current research interest focuses on large-area optoelectronic materials and devices.

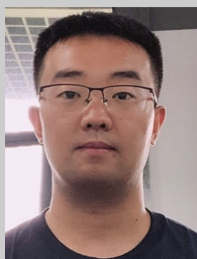

Zuyin Han received his B.S. degree in physics from Shandong University, in 2016. Now he is pursuing his Ph.D. degree in condensed matter physics under the supervision of Prof. Huili Liang and Prof. Zengxia Mei in REL, IOPCAS, and SSLAB. His current research interest mainly focuses on large-area optoelectronic devices based on amorphous gallium oxide.

Zengxia Mei obtained her Ph.D. degree in IOPCAS under the supervision of Prof. Qikun Xue and Prof. Xiaolong Du, in 2005. She joined the faculty of IOPCAS in 2005 and had been working in REL, IOPCAS from 2009 up to 2019. She is currently a professor at SSLAB. Her research interest is defects energetics in functional oxide semiconductors and devices as well as flexible optoelectronic and microelectronic devices.

© 2020 Wiley-VCH GmbH